Exploiting Clausius-Mossotti Factor to Isolate Stages of Human Breast Cancer Cells: Theory and Experiment

Erin Amelia Henslee

Thesis submitted to the faculty of the Virginia Polytechnic Institute and State University
in partial fulfillment of the requirements for the degree of

Master of Science
In
Biomedical Engineering and Sciences

Rafael Davalos
Eva Schmelz
Mark Stremler

January 19, 2010
Blacksburg, VA

Keywords: Dielectrophoresis, Clausius-Mossotti, Breast Cancer

Exploiting Clausius-Mossotti Factor to Isolate Stages of Human Breast Cancer Cells: Theory and Experiment

Erin Amelia Henslee

ABSTRACT

This work demonstrates the ability of contactless dielectrophoresis (cDEP) for isolation of breast cancer cell stages. The ability to selectively concentrate breast tumor cells from a non-transformed or normal cell population is the key to successfully detecting tumors at an early stage of growth and treating transformed cells before they proliferate. Since all cell types have a unique molecular composition it is expected that their dielectrophoretic properties are also unique. DEP force is dependent on the frequency and magnitude of the applied field, as well as a particle's size and electric properties. Specifically, the Clausius-Mossotti factor in the DEP force equation determines a specific cell type's interaction with the electric field and the DEP force response. Cell properties affecting this parameter were investigated numerically and experimentally.

MCF10A, MCF7, and MDA-MB231 human breast cancer cells were used to represent early, intermediate, and late staged breast cancer respectively. Experiments were conducted at 0.02ml/hr with applied voltages of $20V_{rms}$, $25V_{rms}$, $30V_{rms}$, $35V_{rms}$, $40V_{rms}$ and $50V_{rms}$ (n=8). Frequency measurements were recorded for the initial onset of DEP force and when 90% trapping was obtained. The trapping frequency ranges for each cell were distinct from one another with the least amount of overlap between the MCF10A cells and MDA-MB231cells. The MCF7 cell line had, on average, the smallest trapping region at each applied voltage, and fell in between the normal and late staged cells' trapping frequency ranges. Voltages of $20V_{rms}$ to $30V_{rms}$ were found the most efficient for cell isolation.

ACKNOWLEDGEMENTS

I would like acknowledge all of the graduate students and faculty that aided in the production of data, ideas, and suggestions that are contained within this thesis. Thank you first to my advisor Dr. Rafael Davalos for allowing me to be a part of this exciting research and supporting my efforts. I would especially like to acknowledge all the members of the BioElectroMechanical Sysetems (BEMS) Laboratory at Virginia Tech. More specifically I would like to thank all of the support and guidance Hadi Shafiee, Mike Sano, and John Caldwell provided throughout my research. From their creative and brilliant thinking contactless dielectrophoresis became a reality. My sincere thanks goes out to all you for letting me share in this exciting development and being a small part of what will surely be successful and long careers.

To my family, whose support has always been the corner stone to any of my success, all I can say is thank you. I would like to express my deepest appreciation to my husband, William Henslee, who bore the brunt of my late hours and hectic schedule. Finally, I dedicate this thesis to my parents, Mike and Kathy Lennartz, who continue to guide, nurture, and support (not only financially!) my goals and ambition. I would not be where I am today without you.

Table of Contents

Table of Figures

List of Tables

Chapter 1. Introduction

Despite many advances in breast cancer screening and significant survival rate increases since 1990, breast cancer is the most frequent (1 in 8) diagnosed cancer in women in the United States and has the second highest death rate of any other cancer. Currently mammography is the most widely used, efficient method for breast cancer detection [1-2] with studies suggesting an over 90% efficiency rate of accurately detecting cancer [3]. Mammograms, however, cannot detect all forms of cancer, do not guarantee early detection, and have been proven to be less efficient in thin (dense) women as well as women undergoing hormone replacement therapy. In addition are known for false positives resulting in unnecessary biopsies [1-4]. Mammograms are capable of detecting tumors but cannot distinguish between benign and malignant cells and are often too late in preventing malignant tumors from spreading to other parts of the body.

During the early stages of tumor growth, cancer cells that may have exfoliated into bodily fluids (circulating tumor cells, CTCs) could provide early indicators of metastasis [5]. The detection of CTCs or transformed cells from blood samples would enable screening of many types of cancer with one sample. For certain cancers, such as ovarian, prostate and colon cancers, this is especially important since no current screening technique exists. The ability to selectively concentrate these cells is the key to successfully detecting tumors at an early stage of growth and treating transformed cells before they proliferate. In addition, isolation of these cells could provide a workbench for clinicians to screen drug therapies prior to patient treatment. This would enable oncologists to tailor treatment on a patient specific level and to ensure that the most effective treatment is being utilized [6-11].

Carcinogenisis, which is the genetic transformation of normal cells into cancer cells, is a precursor to tumorigensis. Detection of these transformed cells within a population of normal cells is also a promising method for even earlier detection than that by CTCs [12]. Non-tumorigenic cancer cells also undergo genetic transformation thus making detection of transformed cells from normal cells a more encompassing detection technique than CTCs.

CTC's and transformed cells exist at too low a concentration and have too many normal cells present to be detected with existing technologies. Detection techniques such as quantitative polymerase chain reaction (qRT-PCR), immunochemistry and flow cytometry are effective means of verifying the presence of these exfoliated cancer cells under specific conditions. The majority of recent investigations have utilized qRT-PCR for the confirmation and genotyping of CTCs. This technique has been reported in scientific literature as a valid method to confirm various CTCs derived from bladder[13], breast[14], lung[15], prostate[16-17], and esophagus[18]tissues. Immunocytochemistry methods, using antibody-antigen detection, are typically based on detection of specific tumor or epithelial cell markers present in CTCs. While these are reliable methods, the specificity of CTC separation and their enrichment determines the quality of the results. The major drawback to this approach is that other cells, such as hematopoietic or fibroblasts cells, can express several epithelial markers such as keratins as well[19-20] causing an incomplete separation. Current detection techniques generally suffer from a lack of sensitivity, non-specificity, robust presence of inflammatory cells, and tumor heterogeneity. Each of these techniques

relies on different cell properties for separation and has intrinsic advantages and disadvantages. Typically, more sensitive techniques may require prior knowledge of cell-specific markers and antibodies to prepare target cells for analysis. Additionally, the large amount of sample handling required by these techniques greatly increases the likeliness of cell loss and contamination and thus increases the error involved [21].

Dielectrophoresis (DEP) has become a promising technique to separate and identify cells and microparticles suspended in a medium based on their physical and electrical properties. Dielectrophoresis is the motion of a particle in a suspending medium due to the presence of a non-uniform electric field [22-23]. Traditional DEP has been shown to separate breast cancer cells in blood [24-25]. Insulator-based dielectrophoresis (iDEP) exploits the unique intrinsic bioelectrical properties of a cell to differentiate and selectively concentrate cells using insulating obstacles within a microchannel to produce a spatially non-uniform electric field instead of embedded electrodes used in DEP [26]. The BioElectroMechanical Systems (BEMS) laboratory at Virgnia Tech has recently developed a robust, simple, and inexpensive technique, contactless dielectrophoresis (cDEP), to provide non-uniform electric fields in microfluidic channels required for DEP cell manipulation without direct contact between the electrodes and the sample [27]. In this method, an electric field is created in the sample microchannel using electrodes inserted into two conductive microchambers which are separated from the sample channel by thin insulating barriers. These insulating barriers exhibit a capacitive behaviour, and therefore, an electric field can be produced in the main channel by applying an AC field across the barriers [27]. The absence of contact between electrodes and the sample fluid inside the channel prevents bubble formation and avoids any contaminating effects the electrodes may have on the sample. Furthermore, reduced joule heating and a simplified inexpensive fabrication process are the other noticeable advantages of this new technique.

Since all cell types have a unique molecular composition, it is predicted that their dielectrophoretic properties are also unique. It is hypothesized that cDEP technology is capable of isolation and enrichment of breast tumor cells from a non-transformed or normal cell population. By first establishing the dielectrophoretic responses of cells representing early, intermediate, and late stages of breast cancer within cDEP devices, conditions to detect and enrich tumor cells from mixtures with non-transformed cells can be determined.

Chapter 2. Historical Perspective

Approximately 24.6 million people live with cancer worldwide. According to the World Health Organization (WHO), 7.9 million people died of cancer in 2007. Based on projections, cancer deaths will continue to rise with an estimated 12 million people dying from cancer in 2030. Lung, stomach, liver, colon, and breast cancers are the main types leading to overall cancer mortality. In the United States, cancer is the second most common cause of death behind cardiovascular disease, and it accounts for one out of every four deaths. An estimated 40,170 women in the United States were expected to die of breast cancer alone in 2009. Based on the American Cancer Society (ACS) Facts and Figures, the overall cost of cancer to society in 2008 was estimated to be 228.1 billion dollars. If cancer is detected early and if treatment is delivered in a timely, effective manner, survival rates increase significantly. An estimated one-third of all cancers could be cured if detected and treated early.

2.1 Current methods to detect CTCs

Metastatic disease or metastasis occurs when cancer cells break away from the primary tumor into the blood stream or lymphatic vessels and begin to grow in other tissues. Metastasis is one of the primary indicators of malignancy and is considered the cause of most cancer related deaths[21]. Being able to detect and quantify CTCs in peripheral blood or bone marrow can serve many purposes such as providing information on the success or failure of specific therapies and targeting the stage of the disease[28]. The idea that disseminated tumor cells slip into the bloodstream is not new, but the ability to find these few cells among the many millions of blood cells is a relatively recent development. Many attempts to isolate these CTCs from blood have been made for several types of cancers including breast, prostate, renal, and lung.

The majority of recent investigations have utilized RNA-amplification RT-PCR as a sensitive technique for detecting circulating tumor cells. This technique has been reported in scientific literature as a valid method to detect various circulating tumor cells derived from the bladder [13], breast [14], lung[15], prostate[16], and esophagus[18]. RT-PCR is a versatile technique, yet may not be implemented in a clinical setting due to problems associated with reproducibility, high reagent cost, and no clear path to full automation[29].

Immunocytochemistry methods, using antibody-antigen detection, are typically based on detection of cytokeratin present in some types of exfoliated cells, such as squamous cell carcinoma. The major drawback to this approach is that other cells such as hematopoietic cells, can express cytokeratins as well[19]. One of the critical issues that must be addressed, therefore, is the presence of a sufficient number of physically-isolated exfoliated neoplastic cells for this detection methodology to be effective.

These two examples demonstrate the most common problem encountered with current detection techniques: the typical inverse relationship between specificity and sensitivity. If a technology could be developed to overcome the specificity challenge, one would then be free to concentrate solely on sensitivity using protocols and routines already available such as RT-PCR, nucleic acid sequence based amplification (NASBA) or immunocytochemistry. If high-throughput methods to selectively concentrate

and isolate the exfoliated malignant cells in bodily fluids can be developed, it would allow for the detection of precancerous lesions, the early onset of cancer, and/or the detection of micro-metastatic tumors. Early detection of cancer cells, coupled with effective treatment of the disease, would reduce morbidity and mortality associated with the progressive growth of malignancies.

The most reliable method currently available for CTC detection is automated digital microscopy (ADM) which uses image analysis to recognize immunochemically or immunomagnetically labeled tumor cells. The CellSearch System™ (Veridex, LLC; Warren, NJ), as an example, was approved by the FDA in December 2006 as an aid for monitoring patients with metastatic breast cancer. This system involves mixing a blood sample with iron particles coated with an antibody that targets the epithelial cell adhesion molecule (EpCAM). Using this test, Daniel Hayes, M.D. and his colleagues at the University of Michigan Comprehensive Cancer Center reported that the overall survival of patients with breast cancers harboring fewer than five CTCs in about 7mL blood after 3-5 weeks of starting their therapy was a relatively long 18.5 months. Women who had five CTCs or more had much shorter median survival times ranging from 1.3 to 3.6 months [30-31]. Their study tested 177 metastatic breast cancer patients and found patients with fewer than 5 CTCs/7.5ml of blood demonstrated a mean progression free survival time of 7 months. The patients with greater than 5 CTCs/7.5ml of blood had a mean progression free survival time of only 2.7 months. This result was also reflected in the patients' overall survival time of 18 months and 8.2 months respectively[32]. Kurusu et al. assayed for carcinoembryonic antigen (CEA) in peripheral blood from 103 lung cancer patients through reverse transcriptase-polymerase chain reaction. No CEA was detected in control samples. Sixty-two of the 103 patients were positive for CEA in the peripheral blood. Of these 62, 27 remained positive after surgical intervention showing high correlation with pathologic TNM stage of the disease[33]. These results provide proof-of-principle that CTCs are valuable early diagnostic and prognostic cancer markers.

2.2 History of DEP

Dielectrophoresis falls under the umbrella of *electrokinetics* and describes the force interaction between an electric field and a particle's induced dipole. The term dielectrophoresis was created by Pohl in 1951 to describe the movement of particles under dielectric forces (discussed in detail in section 3). Pohl's book in 1978 described DEP in terms of the in-phase dipole force on a neutral particle. The phenomenon was explained as a net force generated on a particle by the interaction between the particles' induced dipole and the applied electric field. When a particle is exposed to an electric field, it polarizes creating a dipole. If the electric field is non-uniform, the electrostatic forces at each pole of the particle are unbalanced creating a net force [34-35]. These early experiments used machined needles to create the non-uniform electric field[36]. Since then the term DEP has been expanded to include all force components including higher order multi-poles and traveling wave DEP[37-38]. Such components include electrorotation in which the DEP force is generated by the dipole lag in a rotating electric field[39-41], electro-orientation in which the induced dipole aligns with the electric field , pearl chaining caused by dipole-dipole interactions [42-46], and as previously mentioned, traveling wave DEP in which the DEP force is generated by the dipole lag in a traveling electric field[26, 47].

Current DEP devices are typically designed around an array of thin-film interdigitated electrodes patterned onto the surface of a substrate within the sample channel. These electrodes generate a non-uniform electric field that interacts with the particles near the surface of the electrode array[48]. Previous work in this area has shown that this traditional DEP is an effective means to concentrate and differentiate cells rapidly and reversibly based on their size, shape, internal structure, and intrinsic properties such as conductivity and polarizability. DEP has proven an efficient, non-invasive method to collect breast cancer cells from a blood sample, to characterize single cells, to detect pathogens, and to manipulate viruses and macromolecules [45, 49-56].

The main drawbacks of the microelectrode-based devices, however, are that they are susceptible to electrode fouling and require expensive, complicated fabrication procedures[36]. In addition since the patterned electrodes at the bottom of the sample channel only create an electric field gradient near their surface, only cells close to the electrodes experience a DEP response thus making these devices unsuitable for high-throughput applications. Typical sample volumes that are processed within these devices are on the order of nano- to microliters, far below that of typical clinical diagnostic sample volumes (mL).

More recently, another method of DEP known as insulator-based DEP (iDEP) was developed[26]. iDEP relies on a DC voltage applied across the sample channel and on the geometry of insulating obstacles within the sample channel to produce electric field non-uniformities instead of the electrode geometry found in traditional DEP. Since these insulating structures typically traverse the entire depth of the channel, a larger area within the sample channel is affected by the electric field gradient greatly increasing device throughput. In addition, the DC field creates electrokinetic flow and moves the solution and particles through the device, alleviating the need for a pump required for a pressure-driven mechanism [57-74]. In iDEP systems, trapping occurs when the DEP force overcomes the electrokinetic force moving the particle. This method however is subject to other disadvantages discussed in section 2.3.

2.3 Development of DEP for CTC detection

An important advantage of DEP to distinguish abnormal cells is that no assumptions regarding their genetic make-up are necessary for the method to be successful. Furthermore, the search strategy relies upon the cells' biophysical properties which are closely aligned with the propensity of the abnormal cell to migrate from its natural environment, an early step in metastatic disease [75]. As opposed to techniques such as fluorescence activated cell sorting (FACS) [76] or pillar-based microfluidic chips [77], no antibody is used in this method for rare cancer cell trapping and identification. Many microchip architectures and configurations have been developed to efficiently sort biological particles by DEP.

The application of DEP to separate target cells from a solution has been studied extensively in the last two decades. Several DEP applications to isolate target cells have been effectively demonstrated including the separation of leukemia, breast cancer and other targeted cells from blood [51-53], cancer cells from CD34+ hematopoietic stem cells [54], neuroblastoma cells from HTB glioma cells [52], cervical carcinoma cells [78], K562 human CML cells[79], mammalian cells based on their cell-cycle phase[55-56], and the separation of cells of the same type based on their activation state [80-81]. In 1992 Gascoyne et al. produced dielectrophoretic characteristics of normal, leukaemic, and differentiation induced

leukaemic erythrocytes from mice as a function of frequency through traditional DEP[82]. Experiments were conducted on an interdigitated gold electrode array of 80μm. Murine erythroleukaemia (MEL) cells were suspended in media and concentrated to 10^5 cells/ml. Mouse erythrocytes were harvested from 0.5ml of blood and resuspended with the MEL cells at a concentration of 10^7cells/ml. The conductivity was adjusted using NaCl to be 2mS/m. A root mean square (rms) voltage of 3V was applied while varying frequency from $5x10^2$ to 10^5 Hz. It was shown that HMBA-treated leukaemic cells had negative collection while untreated leukaemic cells showed positive collection at 22kHz. It was deduced from this that these two cells would separate at that frequency. The same deduction was made for leukaemic cells and healthy cells at 30kHz.

In 1994 this same group published results for separation of both leukemia cells and breast cancer cells from human blood using various DEP methods [24-25]. HL-60 leukaemia cells were suspended with healthy blood cells with a ratio of 2:3. Cells were re-suspended in the same media with $2x10^7$ leukaemia cells and $3x10^7$ normal blood cells. The cell solution had a conductivity of 10mS/m. An interdigiated microelectrode array of 80μm was used once again with glass walls and epoxy cement completing the chamber. Voltage was applied at 5V varying frequency up to 500Hz. MDA231 breast cancer cells were harvested from a pleural effusion and suspended in solution with peripheral blood and T-lymphocytes with a final concentration of $5x10^4$cells/ml. Cells were subjected to a rotating electric field (ROT) and the ROT spectra was measured by timing cell rotation rates (figure 2). A rotating field from 10kHz to 100MHz was applied by sinusoidal waves in phase quadrature to the electrode array.

In this study, the cross over frequencies for HL-60 leukaemic cells, T-lymphocytes, and red blood cells were determined. This frequency was found when (at what frequency) DEP force changed direction. This is an important measurement when determining dielectrophoretic difference amidst different cell types. The crossover frequencies were 180kHz, 320kHz, and 490kHz respectively. From these frequencies, membrane specific capacitance values of 15,11, and $9mF/m^2$ were calculated respectively. Since membrane capacitance is the dominating force in DEP under the given frequencies, this value ultimately determined dielectrophoretic differences in the various cells. The ROT spectra for MDA231 cells, lymphocytes, and erythrocytes along with DEP responses at various frequencies were also determined by this group in 1994[25]. Frequencies of 3, 5.5, and 7MHz caused counter rotation in the respective cells. Crossover frequencies were also found for these cells and were 80, 320, and 450kHz respectively. These measurements showed significant differences in these cells' dielectric properties.

In [83] cell sorting conditions were optimized as well as extended to other forms breast cancer to include: MDA-231, MDA-435, and MDA-468 . Both ROT and DEP techniques were used for this experiment. Concentrations and conductivities of $5x10^4$ cells/ml, 56mS/m and 10^5-10^6 cells/ml, 10mS/m were used respectively. Field frequency for the DEP experiment began at 500kHz at 2V rms to trap all cells and lowered to the frequency predicted by the ROT analysis for optimal trapping of the breast cancer cells. The extent of this work can be seen in Table 1.

Table 1: Results from [24, 82-83] characterizing various cell dielectric properties

Dielectric and Surface Area Parameters for Several Cell Types From ROT Measurements				
Cell Type	r(μm)	C_{spec} (mF/m^2)	Specific area, φ	f_σ/σ_s (MHz m/S)
RBC	2.8±0.1	9±0.8	1	10
T-lymphocyte	3.5±0.2	11±1.1	1.2	6.6
Hepatocyte	10±0.61	80±17	8.9	0.32
DS19	5.9±0.45	17.4±2.0	1.93	2.5
HL-60	5.8±0.42	15±1.9	1.67	2.9
MDA-231	6.2±0.58	25.9±3.7	2.88	1.6
MDA-435	7.7±0.72	13.5±1.9	1.5	2.4
MDA-468	7.2±0.66	27.5±4.2	3.06	1.3

Various new methods employing interdigitated electrodes for DEP have recently evolved including DEP field flow fractionation (fff). Gacoyne et al. used this method for cell separation in 2000[84] as well in later studies including stem cell isolation from adipose tissue in 2008[85].In the 2008 study MDA-435 cells were suspended with hematopoietic CD34+ stem cells, leukocytes, and buffer for a concentration of $5x10^6$ cells/ml. The DEP signal of 4V p-p at 10kHz was applied for 10 minutes to equilibrate cell height. Flow velocity was applied and DEP was then changed to 40kHz releasing T-leukocytes. DEP was then reduced to 5kHz releasing the MDA-435 cells from the electrodes. Their results suggested that breast cancer cells MDA-433 would separate from T-lymphocytes between the frequencies of 20 and 50kHz. Purging breast cancer cells from CD34+ stem cells occurred at ~40kHz. This study extended its application to separation of the major leukocytes from one another (T and B). This separation occurred between 25 and 45kHz.

It has been shown that iDEP is effective for selective trapping of a range of biological particles such as separating and concentrating prokaryotic cells and viruses [61, 68], and sample concentration followed by impedance detection[86]. This technology has shown concentration factors on the order of 6000x and removal efficiencies greater than 98%[61]. So far, iDEP devices have been demonstrated on glass and polymer substrates [58-64, 68-69, 72-73, 87] allowing large electric fields (~10kV/m) to generate eletrokinetic flow and to trap particles. Unfortunately, when used with a highly conductive physiological fluid (such as blood), the relatively high electrical current flow causes dramatic temperature increases due to joule heating and hydrolysis (bubble generation) effects. Additionally, the sample is susceptible to contamination due to direct contact between the electrodes and the sample.

2.4 Development of contactless-DEP(cDEP)

Contactless dielectrophoresis (cDEP) creates electric fields in microfluidic channels required for DEP cell manipulation without direct contact between the electrodes and the sample. In this method, an electric field is created in the sample microchannel using electrodes inserted into two conductive microchambers,

which are separated from the sample channel by thin insulating barriers (Figure 1). In cDEP, AC electric fields are generated in electrodes which are outside of the main microfluidic channel. The electric fields are then capacitively coupled through the substrate, into the main channel with the estimated voltage drop across the main channel given as:

$$\Delta V = \frac{3000 \times f \times V_{external}}{3000 \times f + 15 \times 10^{12} \times \sigma + 10^{6} \times f \times \sigma} \tag{2.1}$$

where f is the applied frequency and σ is the conductivity of the medium. Contactless dielectrophoresis technology eliminates many of the problems associated with traditional DEP and iDEP such as the high fabrication costs, fouling, contamination, bubble formation, and the detrimental effects of joule heating. Varying the insulting structures in all three dimensions has the same effect in cDEP as in iDEP. Since the DEP force on a given particle is frequency dependant, the electric fields generated with cDEP can be used to actively tune a device to capture a specific particle. Another advantage of cDEP is that the field distribution can be changed by changing the configuration of the electrodes.

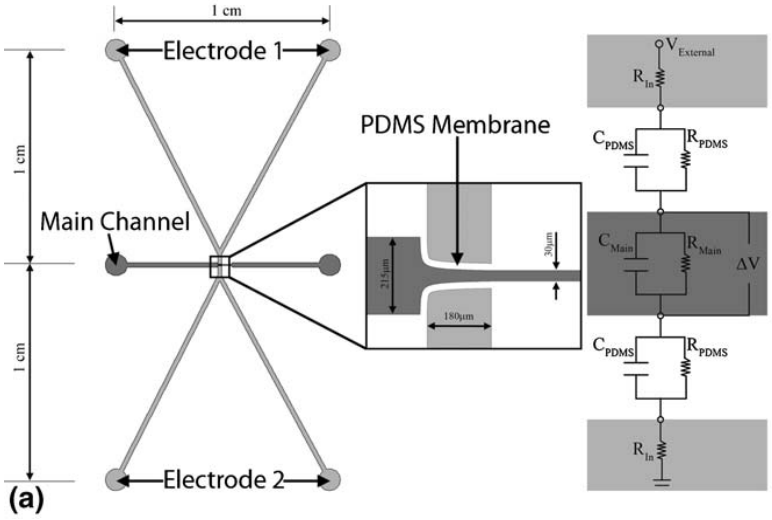

Figure 1: Schematic of original cDEP design with equivalent circuit model. The side channels (electrodes 1 and 2) are filled with a high conductive solution and metal electrodes are inserted into the inlets of each side channel. An AC signal is applied and the thin PDMS membrane acts as a capacitor, generating and electric field across the sample channel[88].

The first cDEP device was developed to observe the DEP response of cells to a non-uniform electric field and was a precursor to the devices used for this study. The effects of different parameters such as total applied voltage, applied frequency, and the electrical conductivity of the fluid inside and outside of the main channel on the resulting DEP response were simulated and then observed through experimentation. DEP responses for three different cell lines (THP-1, MCF-7, and MCF-10A) were observed primarily as a change in cell trajectory or velocity as it traveled through the device. Further evidence of this DEP response to the non-uniform electric field is provided by the electro-rotation of cells and their aggregation in “pearl chain” formations[88].

2.3 Cell lines

For these studies established human cell lines that represent the complete spectrum of the disease were used. Studies began with an established breast cancer progression cell model, the MCF10A system developed by the Michigan Cancer Foundation. MCF10A is a spontaneously immortalized breast epithelial cell line that expresses breast-specific antigens and normal breast epithelial markers such as cytokeratin and milk fat globule antigen but only the modest gene alterations found in cultured cells. MCF10A do not form tumors in mice, thus they will serve as the 'normal' control. The transformation of these cells with k-Ras generated MCF10AT1 cells that form nodules with normal ducts *in vivo* but have been shown to progress to more malignant phenotypes in a subset of immunodeficient mice. The continuous passaging of the cells in mice with selection for tumor formation generated the MCF-10CA1a line that is highly malignant and rapidly forms tumors in mice. This cell system will allow comparison of cells from the same lineage as it could be expected in women after a cell is transformed and progresses into more and more malignant geno-and phenotypes. For the purposes of this study, however, only MCF10A cells will be used as the control cell. Intermediate stages will be represented by the MCF7 cells that express the estrogen receptor and respond to tamoxifen/raloxifen treatment, considered a less aggressive disease genotype. Aggressive, metastatic disease will be represented by the MDA-MB-231 cells.

Chapter 3. Theory

To derive the DEP force acting on a cell, some assumptions must be made about the system. Since the dipole approximation is valid for most electrode configurations except when the particle size and length scale of the nonuniformity of the electric field are of similar size[89], this approximation will be used throughout. Additionally, the cell will be assumed perfectly spherical and be modeled as a lossy dielectric particle.

3.1 Governing equations for a dipole

Consider the dipole in Figure 2. emersed in an electric field with a charge separation $\vec{d}$ a distance $\vec{r}$ from the origin. The net force on this dipole is given as:

$$\vec{F} = q\vec{E}\left(\vec{r} + \vec{d}\right) - q\vec{E}(\vec{r}) \tag{3.1}$$

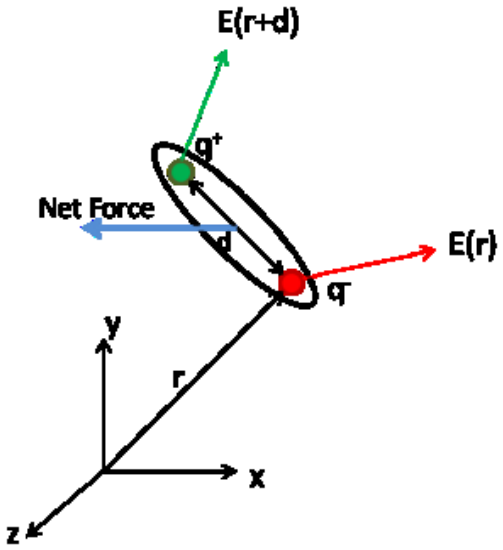

Figure 2: (Adapted from Holmes 2006) The net force on a dipole due to an electric field. This net force will equal zero when E(r)=E(r+d).

Using Taylor series and taking the limit as $|\vec{d}| \to 0$, the dipole approximation can be written as:

$$\vec{F} = q\vec{d} \cdot \nabla\vec{E} = \vec{p} \cdot \nabla\vec{E} \tag{3.2}$$

where $\vec{p}$ is the dipole moment. If the the electric field is uniform ($\nabla\vec{E} = 0$), there is no net force on the dipole. There is, however, a torque (dipole moment) generated by the couple of equal and opposite forces, $q\vec{E}(\vec{r})$ and $q\vec{E}\left(\vec{r} + \vec{d}\right)$ described by:

$$\vec{T} = \frac{1}{2}\vec{d} \times q\vec{E} + \frac{1}{2}\vec{d} \times (-q)\vec{E} = \vec{p} \times \vec{E} \tag{3.3}$$

This dipole moment generates an electrostatic potential where ε_M is the suspending medium permittivity:

$$\Phi = \frac{\vec{p}cos(\theta)}{4\pi\varepsilon_M \vec{r}^2} \tag{3.4}$$

Since the distance between charges, $\vec{d}$, is small compared to the non-uniformity of the electric field, the force and torque can be rewritten and approximated as:

$$\vec{F} \approx \vec{p} \cdot \nabla\vec{E} \tag{3.5}$$

$$\vec{T} \approx \vec{p} \times \vec{E} \tag{3.6}$$

Now consider, instead of a permenent dipole, a dielectric spherical particle with radius R and permittivity ε_p emerged in an electric field with a suspending medium permittivity of ε_M. While the external electric field causes a displacement of charges within the dieletric material, the sphere will have an effect on the electric field inducing an electrostatic potential given by:

$$\Phi_{induced} \approx \frac{(\varepsilon_p - \varepsilon_M)R^3\vec{E} \cdot \vec{r}}{(\varepsilon_p + 2\varepsilon_M)r^3} \tag{3.7}$$

By setting equation 3.4 and 3.7 equal, the expression for the induced (effective) moment can be solved:

$$\vec{p}_{eff} = 4\pi\varepsilon_M K R^3\vec{E} \tag{3.8}$$

where $K(\omega)$ is the Clausius-Mossotti factor and given by:

$$K = \frac{\varepsilon_p - \varepsilon_M}{\varepsilon_p + 2\varepsilon_M} \tag{3.9}$$

To determine the DEP force on a perfectly dielectric (no losses) particle in a non-uniform electric field Figure 3 equation 3.8 can be subsituted into equation 3.5.

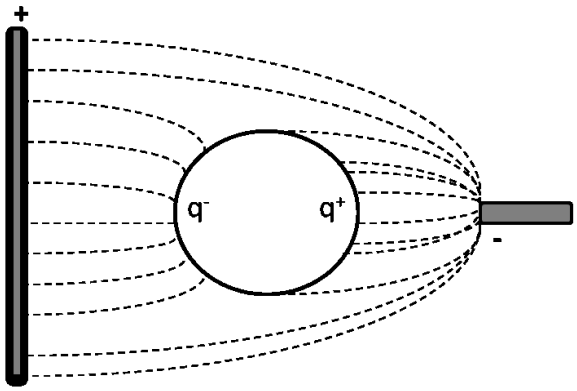

Figure 3: A dielectric particle suspended in a non-uniform electric field.

Using the relation, $\left(\vec{E}\cdot\nabla\vec{E}=\frac{1}{2}\nabla\left|\vec{E}\right|^2\right)$, the DEP force acting on a dielectric, spherical particle can be described by the following [22, 37, 90-91]:

$$F_{DEP}=2\pi\varepsilon_M R^3 K\nabla\left|\vec{E}\right|^2 \tag{3.10}$$

3.2 Clausius-Mossotti Factor

This Clausius-Mossotti factor ranges in value from -0.5 to 1 and in a perfectly dielectric material, in which no losses occur, ε_p and ε_M are scalar values. This is not the case, however, when considering a cell since, at its simplest, a cell model will contain a core and a shell (the membrane) and will not be perfectly insulating. These two key assumptions change the model of the Clausius-Mossotti factor dramatically. Changes in this model are necessary to include since the direction and magnitude of DEP force experienced by a particle is dependent on Clausius-Mossotti.

3.2.1 Theory

First, consider a dielectric (no losses) single shell model (Figure 4) with core radius and permittivity R_2 and ε_1 and outer radius R_1 with shell permittivity ε_2 suspended in a medium of permittivity ε_3. This system can be equilibrated to a particle of radius R_1 with permittivity ε_p. Here ε_p represents the effective permittivity of the combined core and shell.

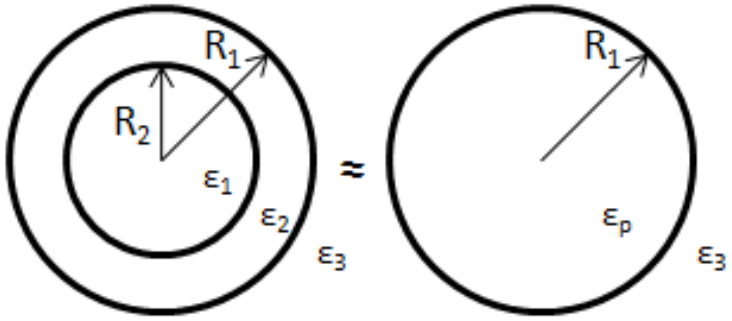

Figure 4: A single shell particle with inner and outer radii R_1 and R_2 respectively and permittivities ε_1 and ε_2 can be modeled equivalently to a particle of radius R_1 with inner effective permittivity ε_p and outer (medium) permittivity ε_3.

Applying this model to a cell of radius R and membrane thickness d with permittivities of the cytoplasm, ε_c and membrane, ε_m, the Clausius-Mossotti factor can be rewritten as:

$$K = \frac{\varepsilon_p^{eff} - \varepsilon_M}{\varepsilon_p^{eff} + 2\varepsilon_M} \tag{3.11}$$

with the expression for ε_p^{eff} given as:

$$\varepsilon_p{}^{eff} = \varepsilon_m \frac{\gamma^3 + 2(\frac{\varepsilon_c - \varepsilon_m}{\varepsilon_c + 2\varepsilon_m})}{\gamma^3 - (\frac{\varepsilon_c - \varepsilon_m}{\varepsilon_c + 2\varepsilon_m})} \tag{3.12}$$

where $\gamma = R/(R-d)$. This process can be repeated for multi-shell models yielding scalar values for Clausius-Mossotti.

If the particle is not perfectly dielectric (lossy), however, electric permittivity must now be considered as a function of frequency where ε_p^* and ε_M^* are the complex permittivities of the particle and the medium respectively. Now the Clausius-Mossotti is written as:

$$K(\omega) = \frac{\varepsilon_p^* - \varepsilon_M^*}{\varepsilon_p^* + 2\varepsilon_M^*} \tag{3.13}$$

where complex permittivity is defined as:

$$\varepsilon^* = \varepsilon - \frac{\sigma}{j\omega} \tag{3.14}$$

where ε and σ are the real permittivity and conductivity of the subject, $j = \sqrt{-1}$, and ω is the radial frequency. The loss is caused by the frequency dependent conductivity term.

The effective complex permittivity of a single shell particle now becomes:

$$\varepsilon_p^{*eff} = \varepsilon_m^* \frac{\gamma^3 + 2(\frac{\varepsilon_c^* - \varepsilon_m^*}{\varepsilon_c^* + 2\varepsilon_m^*})}{\gamma^3 - (\frac{\varepsilon_c^* - \varepsilon_m^*}{\varepsilon_c^* + 2\varepsilon_m^*})} \tag{3.15}$$

Another effect of loss is a phase lag. This lag can derive from the delay of the dipole moment when the field is first switched on and in the case of an AC electric field in which the dipole moment lags behind the harmonically oscillating field (in either case the dipole moment must play "catch up" with the field). The Maxwell-Wagner relaxation time, $\tau_{MW} = \frac{\varepsilon_p + 2\varepsilon_M}{\sigma_p + 2\sigma_M}$, is used to describe the lag present in a *lossy* particle or in a harmonically oscillating field. By introducing the term $\tau_o = \frac{\varepsilon_p - \varepsilon_M}{\sigma_p - \sigma_M}$, the Clausius-Mossotti becomes:

$$K(\varepsilon_p^*, \varepsilon_M^*, \omega) = (\frac{\sigma_p - \sigma_M}{\sigma_p + 2\sigma_M}) \left[\frac{j\omega\tau_o + 1}{j\omega\tau_{MW} + 1}\right] \tag{3.16}$$

Using the complex permitivity definition given in equation (3.14) for the complex permitivitty of a particle in a medium, the real part of Clausius-Mossotti factor is calculated as follows[92]:

$$Re\left[K(\varepsilon_p^*, \varepsilon_M^*, \omega)\right] = \frac{(\sigma_p - \sigma_M)}{(1 + \omega^2\tau_{MW}^2)(\sigma_p + 2\sigma_M)} + \frac{\omega^2\tau_{MW}^2(\varepsilon_p - \varepsilon_M)}{(1 + \omega^2\tau_{MW}^2)(\varepsilon_p + 2\varepsilon_M)} \tag{3.17}$$

The effective permittivity and conductivity of the particle considering a single shell model is given by:

$$\varepsilon_p = \varepsilon_m \frac{\gamma^3 + 2(\frac{\varepsilon_c - \varepsilon_m}{\varepsilon_c + 2\varepsilon_m})}{\gamma^3 - (\frac{\varepsilon_c - \varepsilon_m}{\varepsilon_c + 2\varepsilon_m})} \tag{3.18}$$

$$\sigma_p = \sigma_m \frac{\gamma^3 + 2(\frac{\sigma_c - \sigma_m}{\sigma_c + 2\sigma_m})}{\gamma^3 - (\frac{\sigma_c - \sigma_m}{\sigma_c + 2\sigma_m})} \tag{3.19}$$

where $\gamma = R/(R - d)$; R is the particle radius; d is the cell membrane thickness; ε_c , σ_c and ε_m, σ_m are the complex permitivites and conductivities of the cytoplasm and the membrane, respectively[91-92].

It is important to note that $K(\omega)$ can take both positive and negative values based on the sign of $\varepsilon_p^* - \varepsilon_M^*$. When the particle is more polarizable than the medium ($\varepsilon_p^* > \varepsilon_M^*$), the particle will move toward the region of greatest electric field (positive DEP). If the medium is more polarizable than the particle ($\varepsilon_p^* < \varepsilon_M^*$), however, the electric field will be distorted around the particle inducing the dipole in the opposite direction pushing the particle away from regions of high electric field (negative DEP). The frequency at which $\varepsilon_p^* = \varepsilon_M^*$ and thus $K(\omega) = 0$ is known as the cross-over frequency. By setting $Re(K(\omega)) = 0$ and multplying equation 3.9 by its denominator's complex conjugate the cross over frequency can be calculated:

$$f_c = \frac{1}{2\pi}\sqrt{\frac{-1(\sigma_p - \sigma_M)(\sigma_p + 2\sigma_M)}{(\varepsilon_p - \varepsilon_M)(\varepsilon_p + 2\varepsilon_M)}} \tag{3.20}$$

This frequency can be exploited for dielectric separation of one cell type from a heterogeneous sample.

3.2.2 Model of Clausius-Mossotti factor for cells

When considering a cell in the single shell model, the thickness of the membrane, d, is on a much smaller scale than that of the radius (d<<R). In this case the shell may be modeled in terms of membrane capacitance and conductance is which:

$$\varepsilon_p^{*eff} = \frac{C_m R \varepsilon_p^*}{C_m R + \varepsilon_p^*} \tag{3.21}$$

with $C_m = c_m - j\frac{g_m}{\omega}$. When conductance is assumed to be zero, C_m becomes a noncomplex scalar variable[37, 93]. A parametric study was conducted following the procedure in Docoslis et al.[94] and parameters were adjusted to better suit experimental conditions. As stated in Equation 3.11, the Clausius-Mossotti factor is decribed by:

$$K(\omega) = \frac{\varepsilon_p^{*eff} - \varepsilon_M^*}{\varepsilon_p^{*eff} + 2\varepsilon_M^*}$$

In this model, ε_M^*, the complex permittivity of the medium, is described in Equation 3.14 ($\varepsilon^* = \varepsilon - \frac{\sigma}{j\omega}$) with measured values for the real permittivity and conductivity. The complex permittivity of the cell, ε_p^{*eff}, however, is given as:

$$\varepsilon_p^{*eff} = C_m R[\frac{1 + j\omega\tau_c}{1 + j\omega(\tau_m + \tau_c)}] \tag{3.22}$$

where C_m is the area specific membrane capacitance, τ_c is given as ε_c/σ_c in which ε_c and σ_c are the perimittivity and conductivity of the cytoplasm respectively, and $\tau_m = C_m R/\sigma_c$.
By subtituting Equations 3.14 and 3.22 into 3.11, an expression for the the Clausis-Mossotti factor can be rewritten as:

$$K(\omega) = \frac{\omega^2(\tau_M\tau_m - \tau_c\tau_m^{'}) - 1 + j\omega(\tau_m^{'} - \tau_M - \tau_m)}{2 - \omega^2(\tau_c\tau_m^{'} + 2\tau_M\tau_m) + j\omega(\tau_m^{'} + 2\tau_M + 2\tau_m)} \tag{3.23}$$

with $\tau_M = \varepsilon_M/\sigma_M$ in which ε_M and σ_M are the perimittivity and conductivity of the medium respectively and $\tau_m^{'} = C_m R/\sigma_M$.

A thorough analysis of DEP can be found in [95]. For frequencies below 100 kHz, the imaginary part of the complex conductivity can generally be neglected. At such low frequencies, the applied electric field is primarily dropped across the outer cellular membrane, and the cells behave as poorly conductive spheres. What is important to note here is that cell types having different sizes and/or different membrane dielectric permittivity (which is dominated by cell membrane morphologies, internal conductivities, and size) experience different DEP forces for a given electric field gradient.

Chapter 4. Methods

4.1 Device fabrication

4.1.1 Deep Reactive Ion Etching (DRIE)

Silicon master stamps were fabricated on working grade <100> silicon wafers. Wafers were spun clean at 4,000rpm pouring isopropyl alcohol (IPA) and acetone for 30 seconds, IPA only for 30 seconds, and then spun dry for 30 seconds. The wafers were then placed on a hot plate at 114°C for one minute. A thin layer of Hexamethyldisilazane (HMDS) was spun onto the wafers at 4,000rpm for 1 ½ minutes. AZ 9260 (AZ Electronic Materials) photoresist was spun onto the clean wafers at 500rpm for 25 seconds and 3000rpm for one minute followed by a soft bake at 114°C for 45 seconds (Figure 5:I.a).

A chrome-plated glass mask containing the device designs and the wafer were placed onto the mask aligner. The wafer was then exposed to UV light for 45 seconds at an intensity of 12W/m through the mask. The device channels were filled with chrome on the glass mask exposing the rest of the wafer to the UV light. The exposed photoresist was then removed by placing the wafer into a 3:1 ratio of DI water and Potassium-based buffered developer AZ400K for approximately 2 minutes (Figure 5:I.b). Once washed with DI water, the developed wafers were hard baked at 114°C for one minute.

Deep reactive Ion Etching (DRIE) was used to etch the silicon masters. For a channel depth of 50µm, the DRIE process was set to 20 minutes. This process etches away areas of the wafer where photoresist has been removed leaving elevated channel structures (Figure 5:I.c). Following this process, the wafers are cleaned with acetone to remove any excess photoresist (Figure 5. II). A typical effect of the DRIE etching process is known as the scalloping effect which can create surfaces roughnesses. This roughness can be detrimental to the stamping process as the thin barriers between channels and smaller features of the device could lose their integrity and be torn when removing the copy. To reduce this effect, silicon oxide (SiO_2) was grown on the wafers using thermal oxidation for 4 hours (exposure time may increase with an increased number of wafers) at 1000°C. Once the wafers cooled the silicon oxide was removed with buffered oxide etch (BOE), rinsed with DI water, and placed back into the furnance where the process was repeated.

4.1.2 Polydimethylsiloxane (PDMS) mold

Liquid phase PDMS was made by mixing the PDMS monomers and curing agent at a 10:1 ratio (Sylgard 184,Dow Corning, USA). Each wafer required approximately 50g of the mixture. The PDMS was degassed in a vacuum chamber for one hour. Standard aluminum foil was used to encase each wafer creating a barrier for the liquid PDMS. The PDMS was then slowly poured onto the wafer and upon settling, the wafer was placed under vacuum for 15 minutes. Once all bubbles were removed, the PDMS was then cured for one hour at 100°C (Figure 5:I.f). Lower temperatures to

induce slower curing times were used for devices with smaller features to allow adequate time for the PDMS to settle. Once the wafer was cooled, the aluminum foil was peeled from the PDMS, and the cured PDMS was removed from the wafer. Fluidic inlets and outlets were punched using 1.5mm hole punchers (Harris Uni Core, Ted Pella Inc., Redding, CA) and excess PDMS was cut from the device.

4.1.3 PDMS-Glass Bonding

Both the PDMS mold and glass microscope slides (75mm x75mm x 1.2mm, Alexis Scientific) were cleaned with soap and water, rinsed with DI water, ethanol, IPA, and then dried with compressed air. The PDMS mold was bonded to the glass slide after treating with air plasma for 2 minutes (Figure 5:I.e, III). To increase the bond strength, devices were then placed on a 45°C hot plate for 5 minutes.

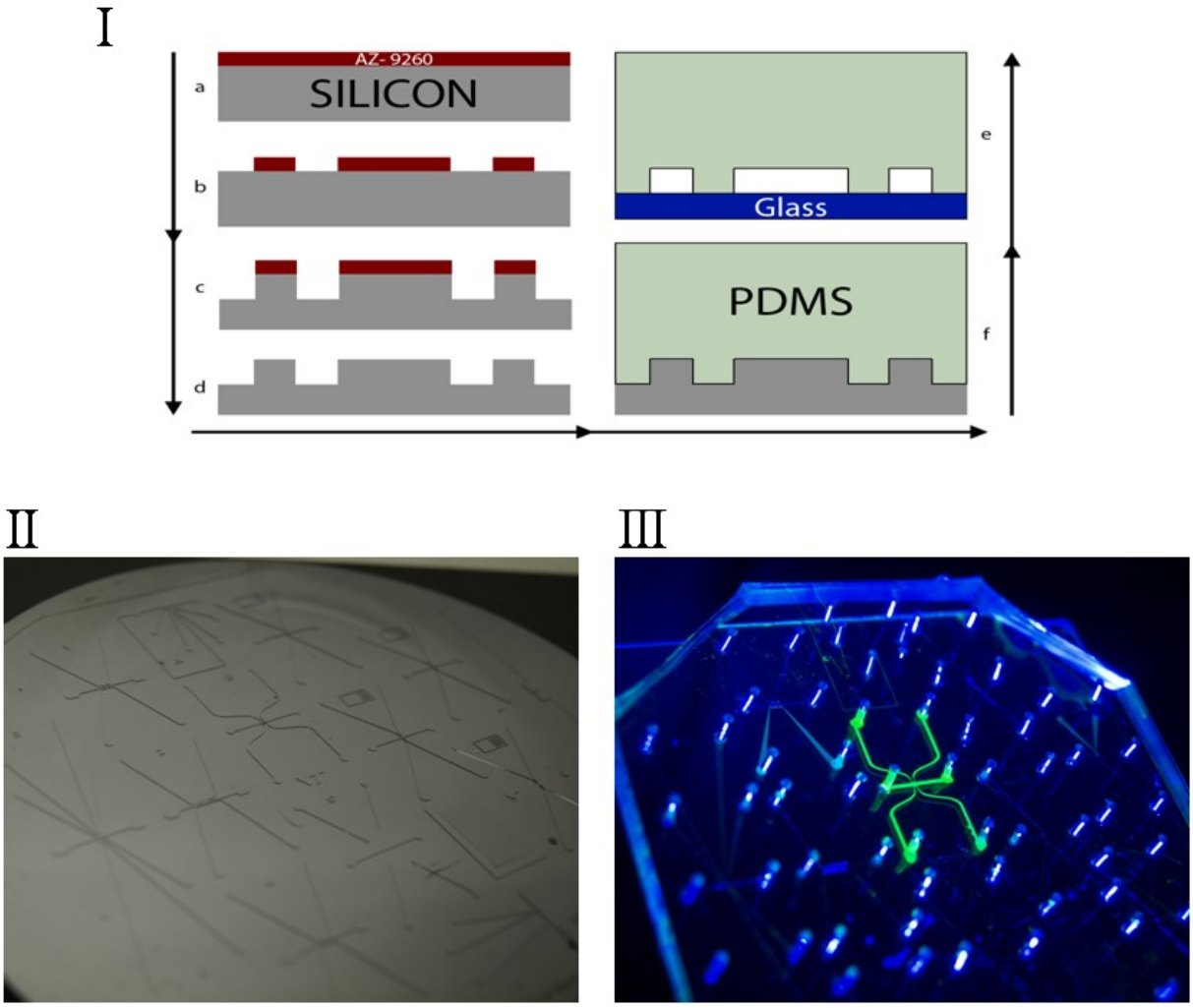

Figure 5: I. (a–e) Schematic of the fabrication process used to create the microfluidic chambers. Steps (a) through (d) are followed only once to create each master stamp. Steps (e) and (f) are repeated to produce an indefinite number of copied devices. II. A completed etched, silicon master stamp. III. A completed PDMS copy, bonded to glass with microfluidic connections. The device of interest is highlighted.

4.2 Cell preparation

4.2.1 Cell Culture

Cells were culutured in DMEM/F12 media (Cellgro, Mediatech, Monassas, VA). The MDA-MB-231 and MCF7 cells were supplmented with 10% fetal bovine serum (FBS) and 1% Penn/Strep. In addition, the MCF7 cells were suppplemented with 0.5nM estradiol and 2ml of 2.5 mg/ml insulin. The MCF10A cells were supplemented with 5% horse serum (HS), 1% Penn/Strep, and 2ml of 2.5 mg/ml insulin, 0.215ml of 50ug/ml EGF, 0.1ml of 2.5mg/ml hydracortisone, and 100ng/ml cholera toxin. All cells were cultured in vented plastic flasks (Corning) at 37^{o} in a 5%CO_2 incubator.

4.2.1 DEP Buffer

To maintain consistent dielectric cell properties, all cells were harvested for experiments at 80% confluency and only maintained to a passage number of 25. After being washed twice with warm Phosphate Buffered Saline (PBS) cells were briefly exposed to 0.25% trypsin-0.02% EDTA. Cells were allocated in two to four 1ml samples and washed twice with sterile DEP buffer (8.5% sucrose [wt/vol], 0.3% glucose [wt/vol] and 0.725% [wt/vol] RPMI)[96]. Cells were centrifuged at 800rpm for 5 minutes. Each ml sample was pipetted with a 300µl pipetter to reduce cell clumping and then combined into a single conical tube for a final concentration of 10^{6}cells/ml. The suspension conductivity of about 110µS/cm was measured with a SevenGo Pro conductivity meter (Mettler-Toledo, Inc., Columbus, OH). If sample conductivity was higher than this, cells were again centrifuged and resuspended.

4.2.2 Cell Staining

To enable simultaneous observation under fluoroscent microscope, MDA-MB 231 cells were stained using calcein AM green while MCF7 and MCF10A cells were stained with CellTrace calcein red-orange AM. Calcein AM is enzymatically converted to green fluorescent calcein by acetoxymethyl ester hydrolysis by intracellular esterases. CellTrace calcein red-orange is intrinsically fluorescent and well retained by live cells. Each stain was added to the cell sample at 2µL per ml of cell suspension. After ten minutes, the cell samples were again washed to remove any excess dye and resuspended in DEP buffer. A one ml sample of each cell was then mixed into one conical tube. Final cell concentrations and conductivities were then measured.

4.3 Experimental Set-up

An inverted light microscope (Leica DMI 6000B, Leica Microsystems, Bannockburn, IL) equipped with color camera (Leica DFC420, Leica Microsystems, Bannockburn, IL) was used to monitor the cell flowing through the main channel.

4.3.1 Syringe pump

Each microfluidic device was placed in a vacuum jar at least 30 minutes prior to experiments to

reduce problems, such as bubble formation, associated with priming. Phosphate Buffered Saline (PBS) was pipetted into the side channels with 300µL pipette tips. With the pipette tips inserted into the inlets of the side channels, aluminum electrodes were then placed in to each. Thin walled Teflon tubing (Cole-Parmer Instrument Co., Vernon Hills, IL) was cut to 8in and 3in and inserted into the inlet (8in tube) and outlet (3in tube) of the main sample channel. A 1 ml plastic syringe containing the cell suspension was then fastened to a micro-syringe pump (Cole-Parmer, Vernon Hills, IL), connected to 20 gauge blunt needles (Howard Electronic Instruments, USA), and then connected to the device inlet tubing. Figure 6 shows a schematic of the experimental set-up. The sample channel was primed with the cell suspension, and the flow rate was set to 0.02ml/hr (equivalent to 222µm/sec for the experimental device) and maintained for several minutes before beginning experiments.

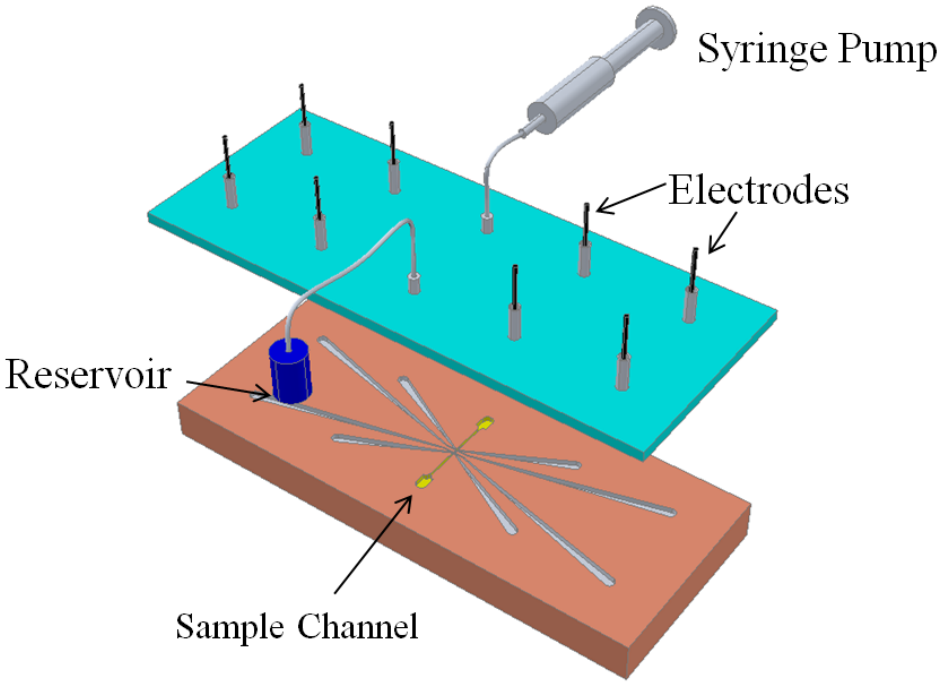

Figure 6: Schematic of device/syringe pump experimental set-up

4.3.2 Electrical Set-up

The electrodes at the top of channel were used for excitation and the electrodes at the bottom of the channel were grounded. Once the flow rate stabalized, AC electric fields were applied using a combination of waveform generation and amplification equipment. Waveform generation was performed by a function generator (GFG-3015, GW Instek, Taipei, Taiwan) whose output was then fed to a wideband power amplifier (AL-50HF-A, Amp-Line Corp., Oakland Gardens, NY). The wideband power amplifier performed the initial voltage amplification of the signal and provided the necessary output current to drive the custom-wound high voltage transformer (Amp-Line Corp., Oakland Gardens, NY). This transformer was placed inside a grounded cage and attached to the

devices using high-voltage wiring. Frequency and voltage measurements were accomplished using an oscilloscope (TDS-1002B, Tektronics Inc. Beaverton, OR) connected to a 100:1 voltage divider at the output of the transformer.

4.3c Safety features

To prevent cellular contamination, all cell culturing and preparation was done under a Thermo Scientific 1300 Series A2 biological safety cabinet. Cells were stored at 37^{o}C in a Thermo Scientific Series 8000-Direct Heat and Water Jacket CO_2 Incubator. Proper guidelines for disposal of cellular waste products were closely followed as well as proper storage for all stains, media components, and experimental devices.

This transformer was placed inside a grounded Faraday cage equipped with a Pinnacle Microguard receiver and attached to the devices using custom made high-voltage leads. To safely monitor voltage, measurements were accomplished using an oscilloscope (TDS-1002B, Tektronics Inc. Beaverton, OR) connected to a 100:1 voltage divider at the output of the transformer. The transformer itself was placed in its own grounded metal enclosure. The wideband power amplifier was equipped with thermal shut down ability.

4.3d Trouble Shooting

During fabrication it was found that at least two layers of silicon oxide (SiO_2) were required for adequate removal of surface impurities. The optimal exposure to air plasma was determined to be 2 minutes on high. To increase the bond strength, the devices were placed on a 45^{o}C hot plate for 5 minutes prior to vacuum.

One of the biggest experimental issues became maintaining a steady flow at low flow rates using the micro-syringe pump. Several attempts at changing tubing length and diameter were made to alleviate this issue. It was found that the longer, smaller tubing was the most successful. However, another issue of cell adhesion within the tubing and at the device inlet had to be balanced with the smaller, longer tubing. To prevent cell adhesion to the tubing and the device, a filtered mixture of 5ml DEP buffer and 50mg BSA was injected into the device and tubing approximately one hour before experiments. This greatly reduced cell adhesion in the device.

During cell preparation the MCF10A's were trypsinized a few minutes longer than the MCF7 and MDA-MB231 cells to remove extracellular components from the cell sample. It was also discovered that the Calcein stains increased the conductivity of the sample, and thus, an extra washing step was added to the cell preparation.

Chapter 5. Numerical Modeling

5.1 Clausius-Mossotti

The DEP spectra, proportional to Clausis-Mossotti, is predicted using Equation 3.23. The parametric study focused on parameters that could not be controlled and measured experimentally (membrane and cytoplasm properties) as well as adjusting experimental conditions such as medium conductivity. The real part of the Clausius-Mossotti was plotted as a function of frequency in MATLAB using a semilog plot. Table 2 lists the nominal parameters used for these plots. Figure 7 demonstrates the sensitivity to experimentally controlled parameters: medium conductivity and particle radius. The sensitivity of the system for these two variables is clearly greater at low and mid-range frequencies ($f<10^8$). Ideally, for the greatest experienced DEP force, the cell would have as large a radius (Figure 7:II.a) as possible suspended in as low conductive solution (Figure 7:I.d) as possible.

Table 2: Nominal parameters used for plot of Clausius-Mossotti.

Nominal Parameter	Value
Radius, (μm)	10
Medium conductivity , σ_M (S/m)	100E-4
Cytoplasm conductivity, σ_c (S/m)	1.3
Membrane Capacitance, C_m (F/m^2)	1.0E-2
Relative Cytoplasm permittivity, ε_c	$60\varepsilon_o$
Relative Medium permittivity, ε_M	$80\varepsilon_o$

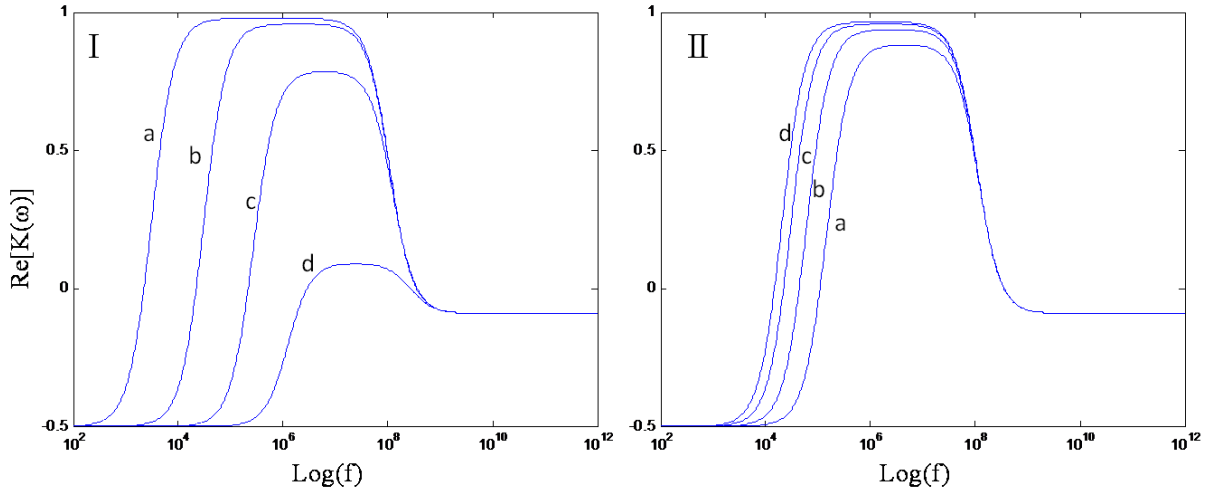

Figure 7: Parametric study of experimentally controlled variables: (I) Medium conductivity (S/m): a. 10E-4, b. 100E-4, c. 1000E-4, and d. 10,000E-4. (II) Particle radius (μm): a. 2, b. 5, c. 10, and d. 15. Nominal parameter values were: σ_M=100E-4 (S/m), r=10(μm), C_m=1.0E-2 (F/m^2), σ_c=1.3(S/m), ε_c=60 ε_o.

In Figure 5 membrane and cytoplasmic properties were varied to determine the sensitivity to possible discrenpencies in these assumed cell parameters. As seen by Figure 8:I, changes in membrane

capacitance are the most significant in lower frequency ranges. Since the electric field can not easily penetrate the cell membrane at lower frequencies, the cell acts as an insulator. At higher frequencies, the electric field can penetrate the membrane, thus the cell acts as a conductor.

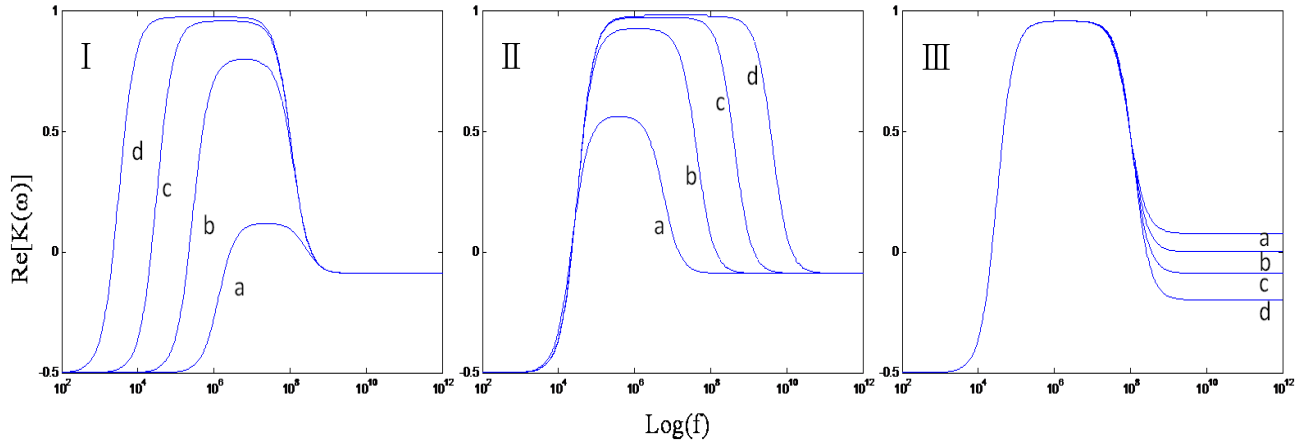

Figure 8: Parametric study of assumed parameters: (I) Membrane capacitance (F/m^2): a. 0.01E-2, b. 0.1E-2, c. 1.0E-2, and d. 10E-2. (II) Cytoplasmic conductivity (S/m): a. 0.05, b. 0.5, c. 5.0 and d. 50. (III) Relative cytoplasmic permittivity: a. 40, b. 60, c. 80, and d. 100. Nominal parameter values were: σ_M=100E-4 (S/m), r=10(μm), C_m=1.0E-2 (F/m^2), σ_c=1.3(S/m), ε_c=60 ε_o.

Figure 8:II shows how changes in cytoplasm conductivity affects the Clausius-Mossotti. This variable has the greatest effect at the mid to high frequency ranges and increases C-M as σ_c increases. Relative permittivity only affects the model at high frequencies, and thus, is negligible in these studies since frequency remains less than 500kHz. In order to amplify DEP force, the difference between the cell and medium electrical properties must be as large as possible.

From Kaler et al.1992[97]the low-frequency cross-over frequency can be determined by:

$$f_c = \frac{1}{2\pi}\frac{\sqrt{2}\sigma_M}{rC_m} \tag{3.24}$$

Experimental data from [94] was able to estimate specific membrane capacitance for viable and nonviable C174 Myeloma cells using Equation 3.24. In addition, σ_c and ε_c were estimated fitting experimental data to Equation 3.23. Their results indicated a large uncertainty in ε_c for both the viable and nonviable cells; however, this discrepency only affected the high frequency ranges of the C-M curves, and thus, is negligble in terms of C-M for this study. Holmes and Morgan used cross-over data to back out the dielectric properties (among them specific membrane capactiance) of human leukemia THP-1 cells[98]. Here the position at which the cell landed on the trajectory electrode was recorded, and from this, DEP force on the cell was determined. Han et al. modeled the cell as a series of parallel RC circuits and was able to obtain membrane specific capacitance for MCF7, MCF10A, MDA-MB231 and MDA-MB435 cell lines[99]. The results from these studies, as well as previously discussed (see Chapter 2) DEP spectra results are summarized in Table 3.

In addition to specific mebrane capacitance, cytoplasm conducivity is a major variable in determining C-M, and therefore is a determining factor in calculating DEP force. According to [100], the cytoplasmic conductivity of a healthy cell is much greater than that of a cancerous cell: 1.31 (S/m) and 0.48 (S/m) respectively. Time domain dielectric spectrometer (TDDS) of static and dynamic

dielectric properties of normal and malignant blood cells were determined by [101] with a lower and upper limit of cytoplasm conductivity of 0.033 (S/m) and 1.1 (S/m) respectively. Internal conductivity of MDA-MB231 cells was found to be 0.62±0.073(S/m) from parameter optimization of ROT spectra[102].

Table 3: Dielectric parameters of various cancerous and noncancerous cells

Cell Type	$r\ (\mu m)$	$C_m\ (mF/m^2)$	
RBC	2.8 ± 0.1	9±0.8	Source: [24, 82-83]
T-lymphocyte	3.5±0.2	11±1.1	
Hepatocyte	10 ±0.61	80±17	
DS19	5.9±0.45	17.4 ±2.0	
HL-60	5.8±0.42	15±1.9	
MDA-MB231	6.2±.58	25.9±3.7	
MDA-MB435	7.7±0.72	13.5 ±1.9	
THP-1	6.4 ± 1.0	17.7±2.7	Source: [98]
C174 Viable	8.18± 0.42	14.8±0.3	Source: [94]
C174 Nonviable	5.0±1.0	13.0+± 1.0	
MDA-MB435	n/a	15.7±1.2	Source:[99]
MDA-MB231	n/a	16.3±1.7	
MCF7	n/a	18.6±1.1	
MCF10A	n/a	19.4± 1.4	

The real part of the Clausis-Mossotti factor was plotted as a function of frequency for MDA-MB231, MCF7, and MCF10A using MATLAB with parameters shown.

MCF10A	Value
Radius, (μm)	9.1
Medium conductivity ,σ_M (S/m)	100E-4
Cytoplasm conductivity, σ_c (S/m)	1.0
Membrane Capacitance, C_m (F/m^2)	1.94E-2

MCF7	Value
Radius, (μm)	9.25
Medium conductivity ,σ_M (S/m)	100E-4
Cytoplasm conductivity, σ_c (S/m)	0.75
Membrane Capacitance, C_m (F/m^2)	1.86E-2

MDA-MB231	Value
Radius, (μm)	8.93
Medium conductivity ,σ_M (S/m)	100E-4
Cytoplasm conductivity, σ_c (S/m)	0.48
Membrane Capacitance, C_m (F/m^2)	1.63E-2

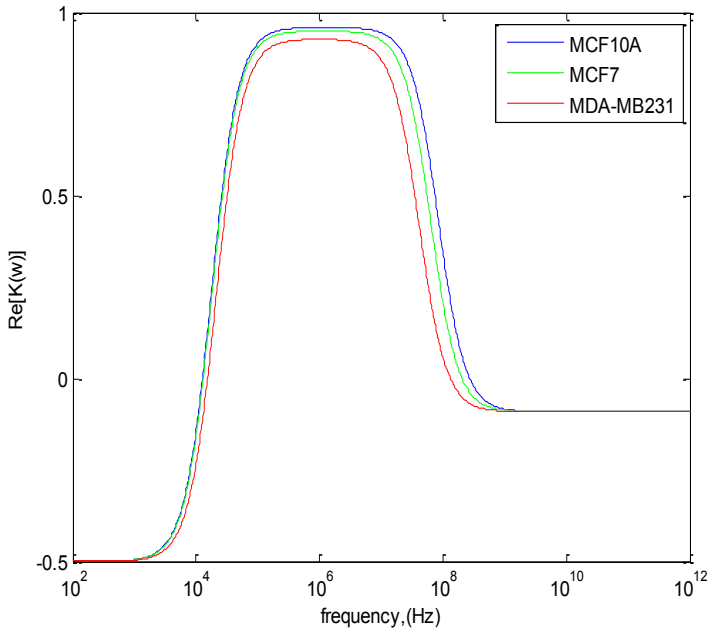

Figure 9: The real part of Clausius-Mossotti for MDA-MB231, MCF7, and MCF10A and estimated parameters.

Cytoplasmic conducitivty for the normal MCF10A cells was set to 1 (S/m) as a standard for comparison for the cancer lines. MDA-MB231 was given the low end of the spectrum value of 0.48 (S/m), and MCF7 was set to a median value of 0.75 (S/m).

Though the margin of variation between the viable cells is small, the frequency region with the greatest variation was between 10^4 and 10^6 (Hz), the same region in which experimental trials will be conducted (on the order of 10^5 (Hz)). Assuming the cells are exposed to the same electric field at a given location within a device, the estimated response to DEP can be determined by normalizing the gradient to 1 and multiplying Clausius-Mossotti by $2\pi r^3$ for each cell line. Figure 10 shows that the response differences of the cells is now increased. This is a positive indicator of the ability to isolate one cell population from another using the experimental set-up and cDEP designs described in this study.

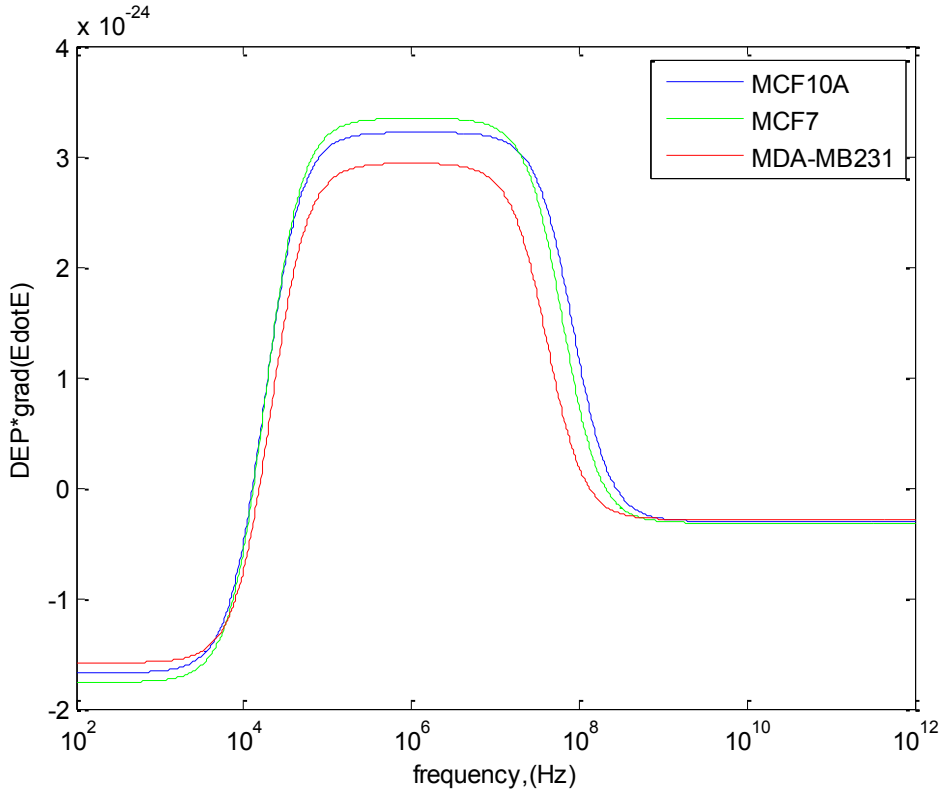

Figure 10: Estimation of DEP force with a normalized electric field gradient.

5.2 Model of cell in electric field

An important aspect in predicting DEP response of various cells is how the individual cell properties affect the electric field and vice versa. As stated previously, when the particle is more polarizable than the medium ($\varepsilon_p^* > \varepsilon_M^*$), the particle will move toward the region of greatest electric field (positive DEP). If the medium is more polarizable than the particle ($\varepsilon_p^* < \varepsilon_M^*$), however, the electric field will be distorted around the particle inducing the dipole in the opposite direction pushing the particle away from regions of high electric field (negative DEP). More importantly in terms of cell isolation and separation, however, is how polarizable cells are compared to one another. More specifically, the differences between cancerous and noncancerous cells are needed for applications in this study. A 10μm cell suspended in a medium between two plates was modeled in COMSOL Multiphysics to demonstrate this principle (Figure

11). Medium conductivity was 0.1(S/m) while the top plate was given a potential of 10V and the bottom plate was set to ground at a frequency of 200kHz.

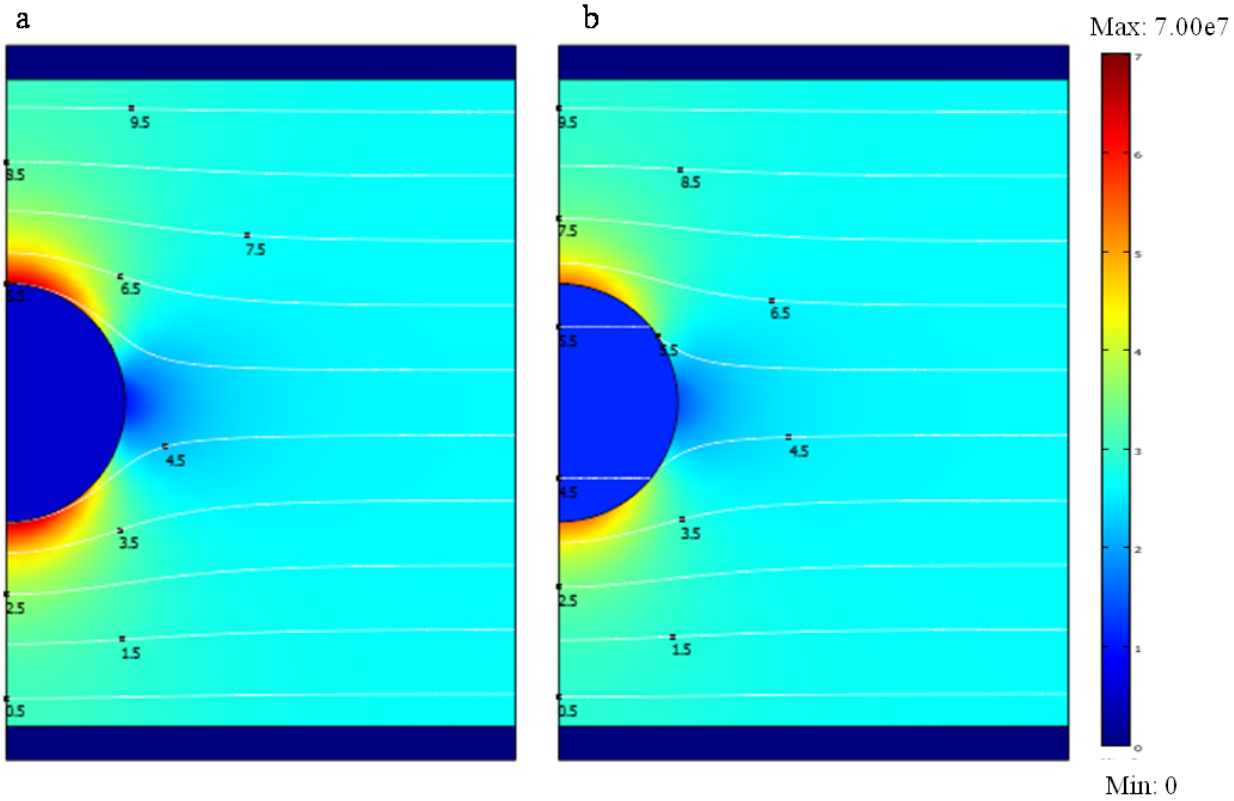

Figure 11: Comsol model of a cell suspended in an electric field. A surface plot of the electric field for: a. normal cell parameters and b. cancerous cell parameters

Cell parameters were taken from [100] and listed below in Table 4. Clearly, there is a much higher electric field generated at the poles of the normal cell indicating that the normal cell is more polarizable than the cancerous cell. This coincides with results discussed in section 5.1 as the capacitance (ability to store charge) is much higher in a normal cell compared to its cancerous counterpart. As cancer progresses, the membrane becomes more permeable (as seen in Figure 11b).

Table 4: Cell parameters for COMSOL model

	Normal	**Cancer**
Conductivities (S/m):		
Medium, σ_M	0.01	0.01
Membrane, σ_m	5.60E-05	9.10E-06
Cytoplasm, σ_{cyt}	1.31	0.48
Relative Permittivity:		
Medium, ε_M	$80\varepsilon_o$	$80\varepsilon_o$
Membrane, ε_m	$12.8\varepsilon_o$	$9.8\varepsilon_o$
Cytoplasm, ε_{cyt}	$60\varepsilon_o$	$60\varepsilon_o$

The ultimate goal in particle separation is to achieve both positive and negative DEP response. For instance, for the best possible selectivity, the cell of interest should be trapped (positive DEP) to insulating structures, while background particles, such as blood particulate, are pushed away (negative DEP) from insulating structures. This model is a good indicator of polarizability and permeability, each of which affect whether positive or negative DEP is being observed.

In addition, this model was used to observe the effects of frequency on the cell. Normal cell parameters were maintained while frequency ranged from 200kHz to 100MHz. It should be noted the cell nucleus is an insignificant factor until high frequency ranges (f>1MHz)[103]. No significant changes were observed in the electric field increasing frequency until 1MHz.

5.3 Device modeling

Two devices were modeled following the procedure in [104]. The electric field distribution and its gradient $\nabla E = \nabla(\nabla\emptyset)$ were modeled numerically in Comsol multi-physics 3.5 using the AC/DC module (Comsol Inc., Burlington, MA, USA). This is done by solving for the potential distribution, ϕ, using the Laplace equation, $\nabla \cdot (\sigma^*\nabla\emptyset) = 0$, where σ^* is the complex conductivity ($\sigma^* = \sigma + j\omega\varepsilon$) of the sub-domains in the microfluidic devices. The boundary conditions used are prescribed uniform potentials at the inlet or outlet of the side channels.

The values for the electrical conductivity and permittivity of the PDMS, PBS, and DEP buffer that were used in this numerical modeling are given in [104]. PBS and DEP buffer electrical properties are used for the side and main microfluidic channels, respectively. The induced DEP effect inside the main channel was investigated for a range of frequencies and voltages.

From these models predictions of trapping location and ability of each device can be determined since DEP force is dependent on the gradient of the electric field. Figure 12.a and Figure 13.a indicate the areas of high electric field gradient within each channel (see contour lines), and thus, the location of potential trapping (where the contour lines are bright red). Additionally, the forces acting on the particle in the microfluidic device are shown in Figure 12 and Figure 13. For particles larger than 1 μm, the Brownian motion is negligible compared to the DEP force[91]. The parabolic velocity profile in the microchannel is due to the low Reynolds number pressure driven flow across the main channel. Assuming the cell as a spherical particle, the hydrodynamic drag force due to cell translation is given by:

$$f_{Drag} = 6\eta r\pi(u_p - u_f) \tag{5.1}$$

where *r* is the particle radius, η is the medium viscosity, u_p is the velocity of the particle, and u_f is the medium velocity. The velocity of the particle is determined by a balance between the DEP force and Stoke's drag force. The relationship is given by:

$$u_p = u_f - \mu_{DEP}\nabla(E \cdot E) \tag{5.2}$$

where μ_{DEP} is the dielectrophoretic mobility of the particle and is defined as:

$$\mu_{DEP} = \frac{\varepsilon_M r^2}{3\eta} Re[f_{CM}] \tag{5.3}$$

For the experimental cells with diameters greater than 10μm, the charachteristic time for a particle suspended in a fluid , given by $\frac{2\rho r^2}{9\eta}$ is about 10^{-4} s, orders of magnitude smaller than the time scale of the external forces and our experimental observations thus the acceleration term in in the force balance equation can be neglected[105-106]. Additionally, since DEP and hydrodynamic drag forces are acting in the horizontal plane, the gravitational force is negligble compared to these aformentioned forces in DEP cell manipulation.

These devices were designed using finite element modeling in order to provide a strong enough gradient of the electric field for THP-1 cell separation and enrichment. The gradient of the electric field along the center line of the main channel of the devices is plotted in Figure 12(b-c) and Figure 13(b-c). These numerical results indicate that the gradient of the electric field, and thus the DEP effect, is strongly related to the channel geometry. The insulator-based design (Figure 13) was determined to be the most selective (see Chapter 6), and thus, was chosen for breast cancer cell isolation. Maximum gradient of the electric field along the x (y=0) and y (x=0) axis of of this device for frequencies between 200kHz and 10,00kHz were modeled in COMSOL (Figure 14).

Knowing the velocity of the sample fluid, the maximum gradient of the electric field given by Figure 14, and the particle's DEP mobility determined by Equation 5.3, it can then be determined if a device design is capable of cell trapping ($u_p = 0$). To tailor designs towards trapping a particular cell from a heterogeneous sample, cell properties can be used to determine the electric field gradient necessary for the cell to trap while the velocity of the other particles/cells is nonzero. One of the biggest advantages of cDEP is the ability to manipulate this gradient by varying the electrode configurations and the insulating structure design.

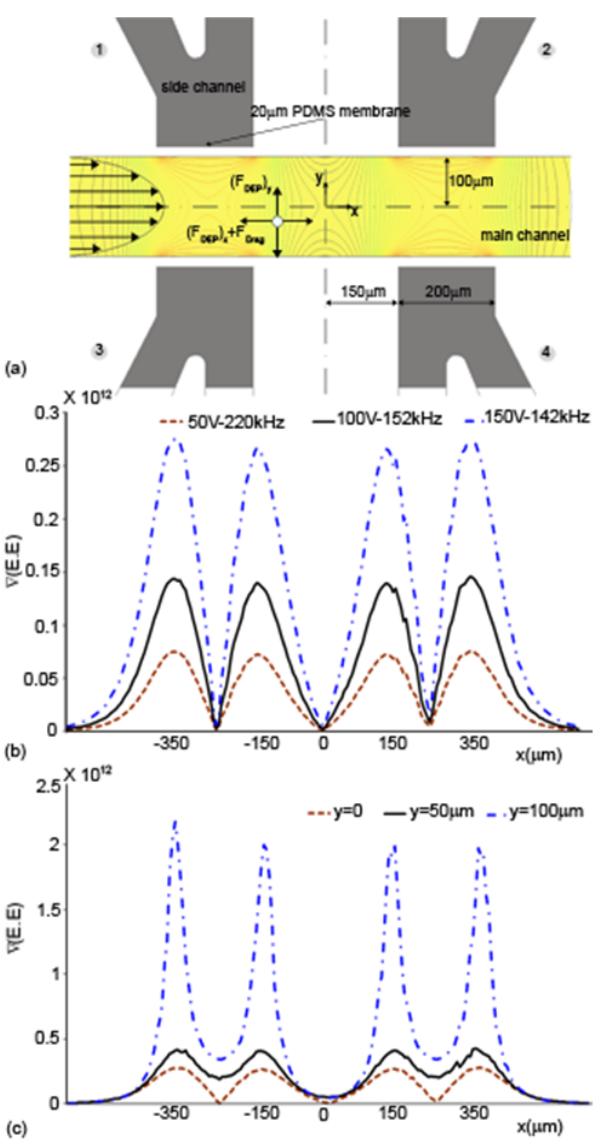

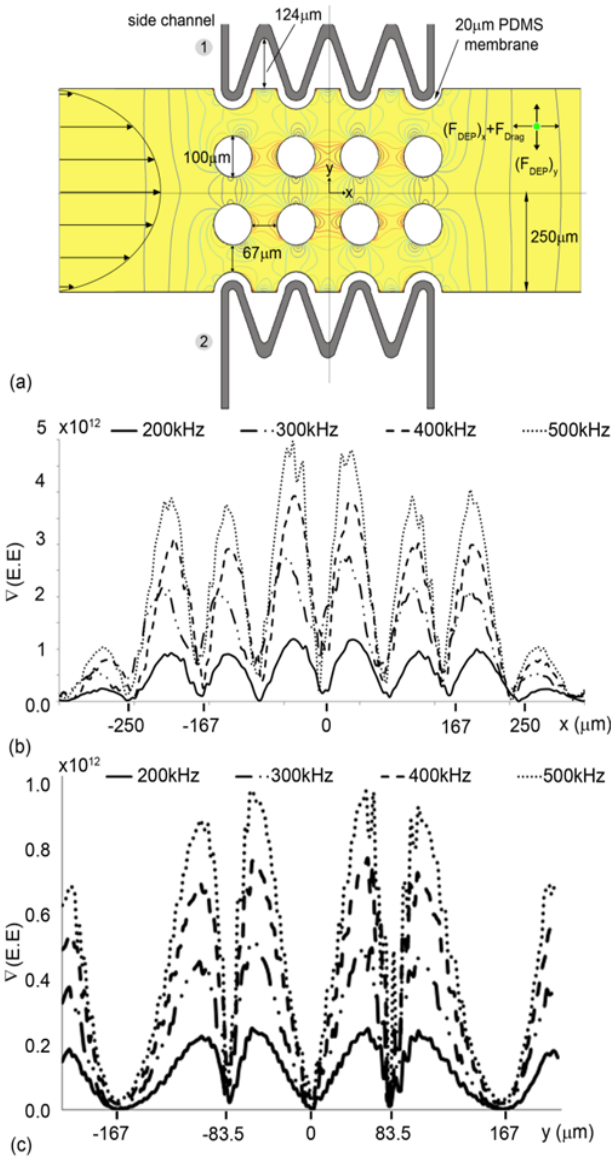

Figure 12: (a) 2D top view schematic of the first experimental device showing the dominat acting forces on the particle. The contours represent the electric fields. (b) Line plot of the gradient of the electric field squared (kg^2 m C^{-2} S^{-4}) for three different electrical boundary conditions with efficient numerical cell trapping (V1=V2=50Vrms at 220 kHz, 100Vrms at 152kHz, and 150Vrms at 140kHz and V3=V4=Ground). (c) Line plot of the gradient of the electric field squared (kg^2 m C^{-2} S^{-4}) along the lines parallel to the center line of the main channel and at different distances from the channel wall for V1=V2=150Vrms at 140kH boundary condition (y=0, 50, and 100μm).

Figure 13: (a) 2D top view schematic of device 2 showing the dominated acting forces on the particle. The contours represent the electric fields. (b) Line plot of the gradient of the electric field squared (kg^2 m C^{-2} S^{-4}) for four different electrical boundary conditions with efficient numerical cell trapping (V1=30Vrms at 200kHz, 300kHz, 400kHz, and 500kHzV2= Ground) along the x axis (y=0). (c) Line plot of the gradient of the electric field squared (kg^2 m C^{-2} S^{-4}) for four different electrical boundary conditions with efficient numerical cell trapping (V1=30Vrms at 200kHz, 300kHz, 400kHz, and 500kHz, and V2= Ground) along the y axis (x=0).

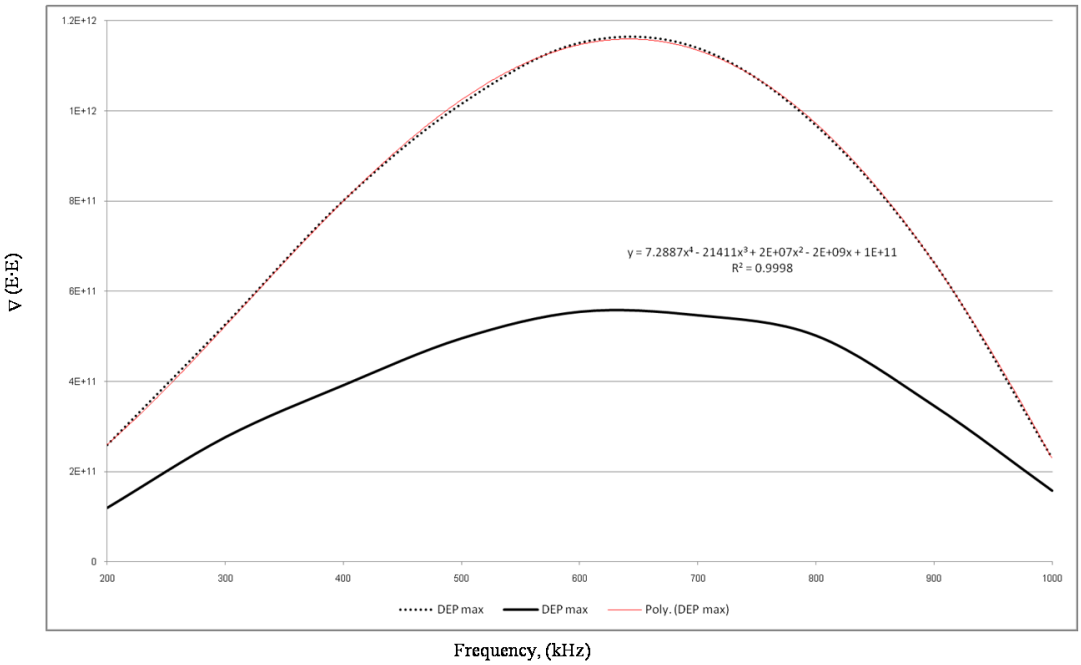

Figure 14: Maximum gradient of the electric field along the x (y=0) and y (x=0) axis of device 2 for frequencies between 200kHz and 1000kHz. The red line is the polynomial curve fit to the numerical data.

Chapter 6. Results and Discussion

6.1 Examining the abilities of cDEP: Live/Dead THP-1 isolation

The ability of cDEP to selectively isolate and enrich a cell population was first investigated through designing and testing a second generation of cDEP devices [107]. This was demonstrated through the separation of viable cells from a heterogeneous population also containing dead cells. Human leukemia THP-1 viable cells were successfully isolated from nonviable cells treated with hyperthermia. Optimization of these devices would allow for the selective separation of cells from biological fluids for purposes such as: the diagnosis of early stages of diseases, drug screening, sample preparation for downstream analysis, enrichment of tumor cells to evaluate tumor lineage via PCR, as well as treatment planning. By using viable/nonviable separation as a model for these applications, a new generation of cDEP devices can be tailored around the results reported in this study.

6.1.1 Cell Preparation and Experimental Set-up

The live samples of THP-1 human leukemia monocytes were washed twice and resuspended in our prepared DEP buffer (8.5%sucrose [wt/vol], 0.3% glucose [wt/vol], and 0.725% [wt/vol] RPMI) [96]. The cell samples to be killed were first pipetted into a conical tub and heated in a 60^{o}C water bath for twelve minutes, an adequate time determined to kill a majority of the cell sample. The dead cells were then washed twice and resuspended in the DEP buffer.

To enable simultaneous observation under fluorescent microscope, cells were stained with fluorescent dye of LIVE/DEAD® Viability/Cytotoxicity Kit for mammalian cells (Molecular Probes Inc.). Calcein AM, which is enzymatically converted to green fluorescent calcein, was added to the live cell sample at 2μL per ml of cell suspension. Ethidium homodimer-1 (EthD-1) was added to the dead cell sample at 6μL per ml of cell suspension. It can only pass through damaged cell membranes and upon nucleic acid-binding, it produces a red fluorescence. The two samples were then vortexed for 5 minutes, washed once and resuspended in DEP buffer. The live and dead suspensions were then mixed together in one conical tube, and the final conductivity of 115μS/cm was measured with a Mettler Toledo SevenGo Pro conductivity meter (Mettler-Toledo, Inc., Columbus, OH).

6.1.1 Experimental Results

Live THP-1 cells were observed to experience a positive DEP force at the reported frequencies, and the DEP force applied on dead cells appeared to be negligible. Trapping efficiencies greater than 90% at all tested frequencies (200 kHz, 300 kHz, 400 kHz, and 500 kHz) were observed. The concentration of live THP-1 cells using a 150 kHz voltage signal at 100 V_{rms} in the device without posts is shown in Figure 15. The same experimental results for the insulator based device with a 500 kHz, 40 V_{rms} signal is shown in Figure 16. Under these parameters, the DEP force on the dead cells was not sufficient to influence their motion, and they passed through the trapping region. The enriched sample of live cells can be controllably released for later analysis once the electric field is turned off (Figure 15.c and Figure 16.c). The cells continued to fluoresce indicating that they remained viable.

This work has demonstrated the ability of cDEP to selectively concentrate specific cells from diverse populations through the separation of viable cells from a sample containing both viable and nonviable human leukemia cells. For an in depth discussion of these live/dead results refer to [104].

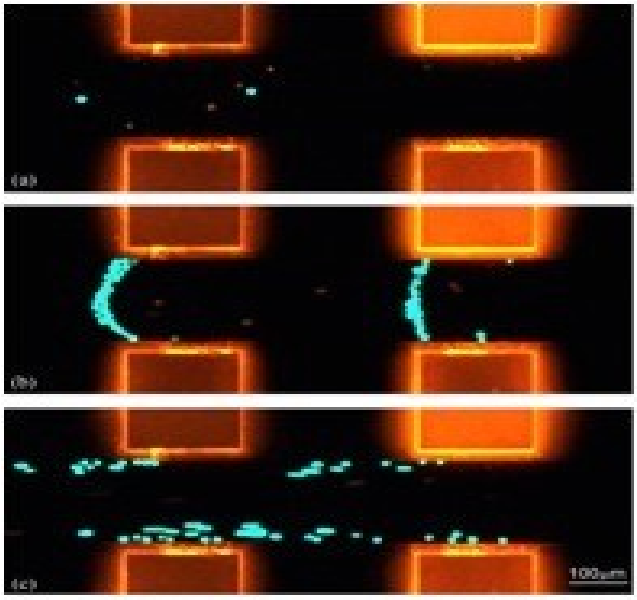

Figure 15: (a) Dead (red) and live (green) THP-1 cells are moving from right to left due to pressure driven flow without applying electric field. (b) 30 seconds after applying the field (Top 100V_{rms} at 152 kHz and Bottom=Ground). The live (green) cells are trapped due to positive DEP, but the dead (red) cells pass. (c) Releasing the trapped live cells by turning off power

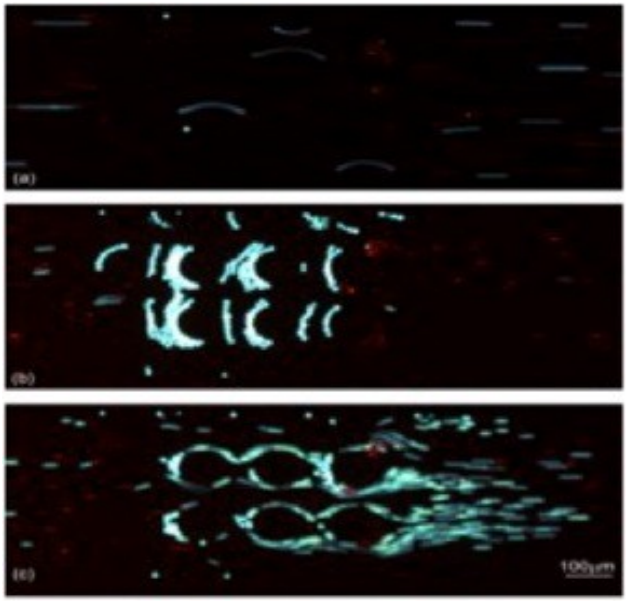

Figure 16: Experimental results for insulator based device: (a) Dead (red) and live (green) THP-1 cells are moving left to right due to pressure driven flow. (b) 30 seconds after applying the electric field (V1=40 V_{rms} at 500 kHz and V2=Ground) live cells were trapped due to positive DEP but dead cells pass by. (c) Releasing the trapped live cells by turning off the power supply.

6.2 Ability of cDEP for isolation of breast cancer stages

Numerical results indicated that the insulator based design provided much higher electric field gradients, and thus, was the focus for this investigation. Once sufficient trapping (90%+) was observed for all cell lines in the device, separately heterogeneous samples of MDA-MB231 and the MCF cells were examined in the device. Experiments were conducted at 0.02ml/hr with applied voltages of 20V_{rms}, 25V_{rms}, 30V_{rms}, 35V_{rms}, 40V_{rms} and 50V_{rms} (n=8). Frequency measurements were recorded for the initial onset of DEP force (noticeable movement of the cells toward the insulators) and when 90% trapping was obtained (an example of this is given in Figure 17). As seen in Figure 19, the trapping regions for each cell were distinct from one another with the least amount of overlap between the MCF10A (normal) cells and MDA-MB231 (late staged) cells. The MCF7 cell line (intermediate) had, on average, the smallest trapping region at each applied voltage, and fell in between the normal and late staged cells' trapping regions. Another interesting discovery was that the amount of overlap between the frequency trapping region of each cell line increased as higher voltages were applied, suggesting that for this device voltages of 20V_{rms} to 30V_{rms} are the most efficient for cell isolation.

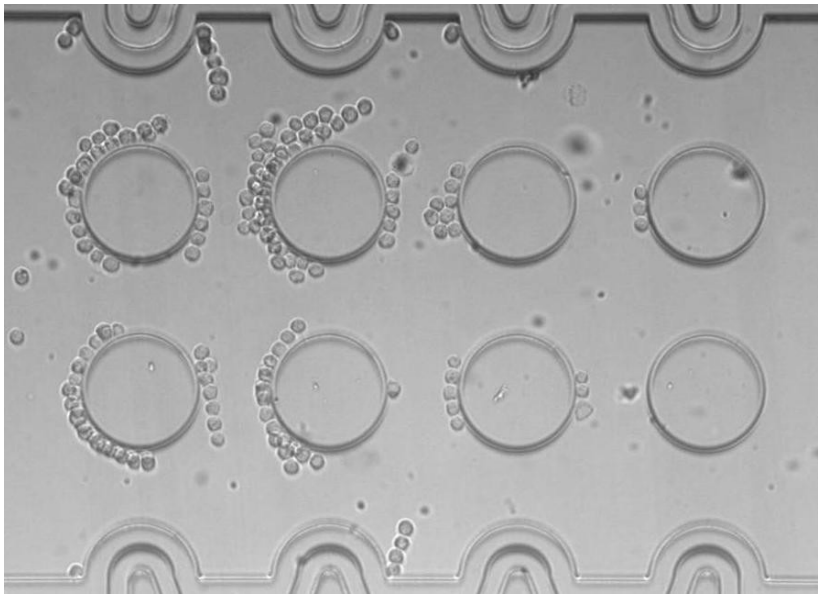

Figure 17: Experimental image of 90% trapping of MCF10A breast cancer cells at 30V and 290kHZ

Additionally, it is clear from Figure 18 and Figure 19 that the MCF10A cells required a much higher frequency for DEP observed responses than that of the highly metastatic MDA-MB231 cells. This deviates from the numerical predictions that cancerous cells are more conductive and thus less polarizable than normal cells. This suggests other membrane properties aside from membrane capacitance must play a major role in dielectric response of a cell.

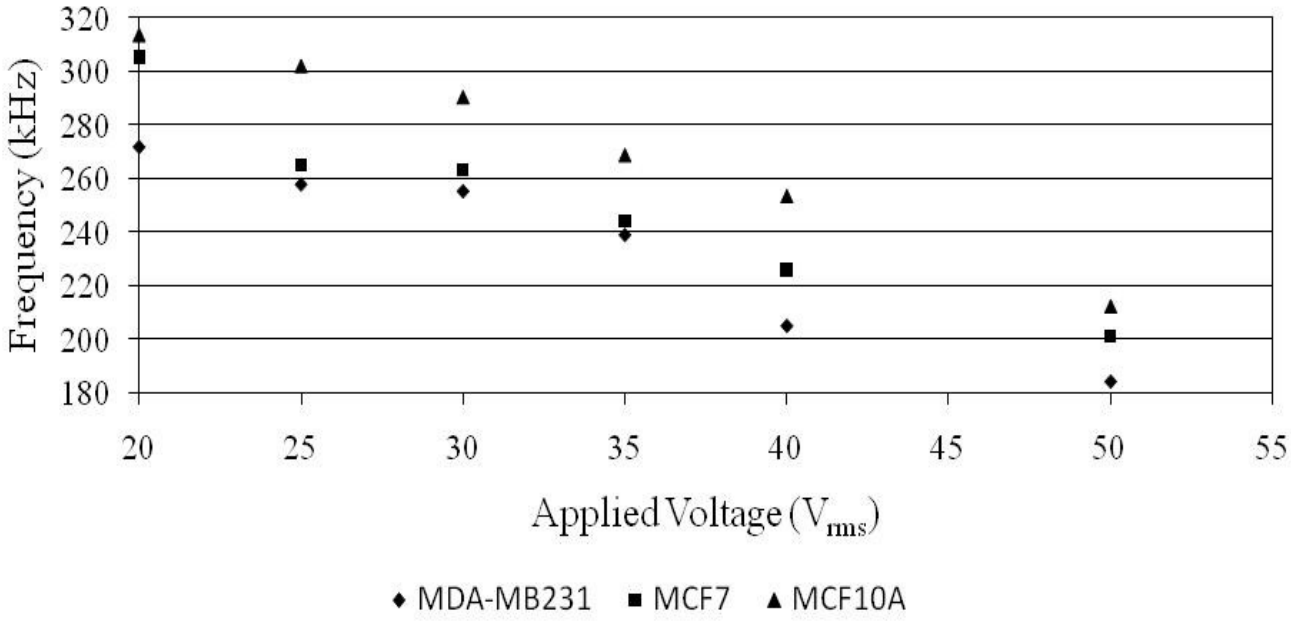

Figure 18: Frequency required for 90% trapping at: 20Vrms, 25Vrms, 30Vrms, 35Vrms, 40Vrms and 50Vrms for MDA-MB231, MCF7 and MCF10A cells.

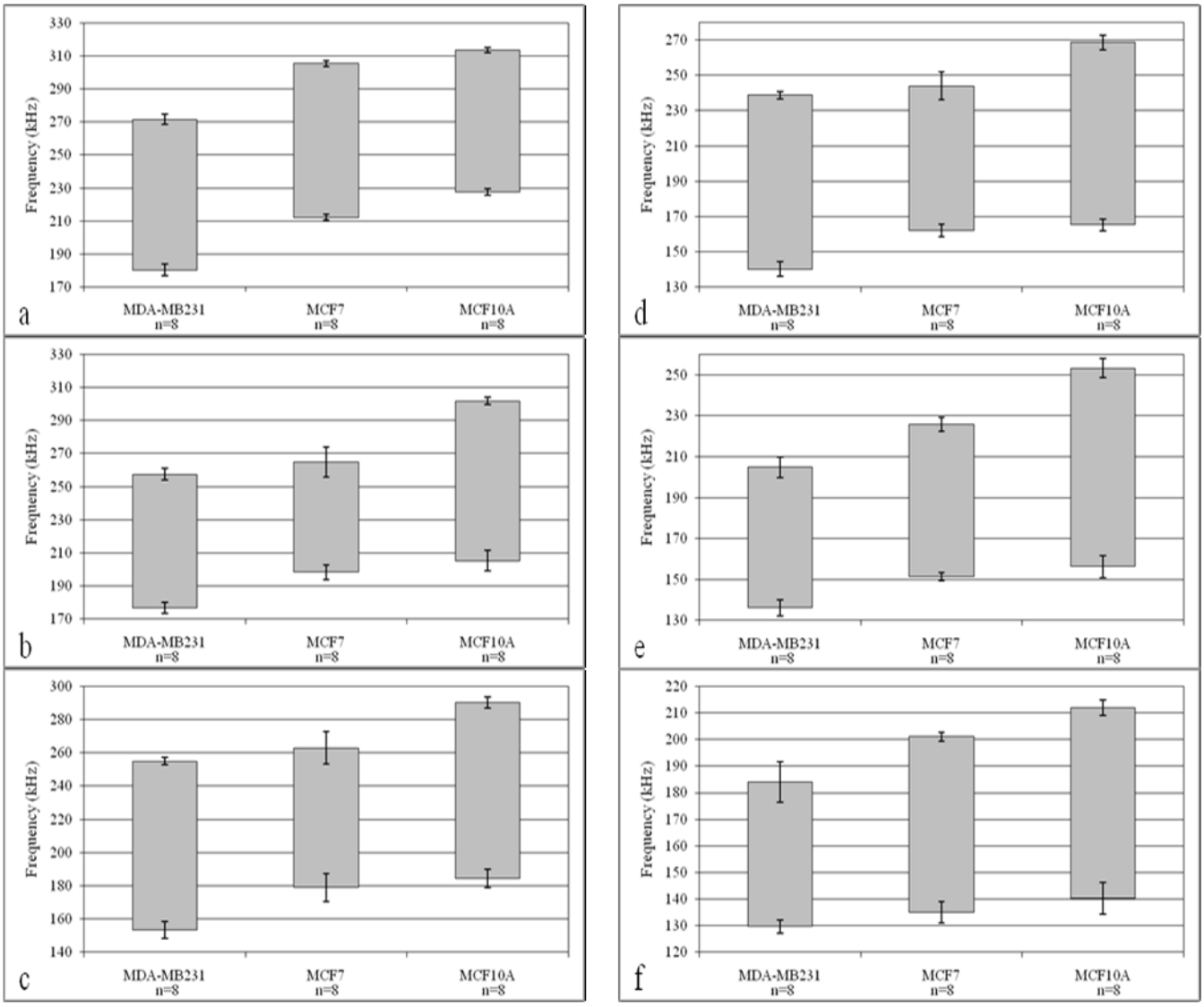

Figure 19: Trapping conditions for MDA-MB231, MCF7 and MCF10A breast cancer cells from initial DEP response until at least 90% trapping was achieved. Frequencies were recorded for initial DEP response and 90% trapping for each cell at 6 different applied voltages: a. 20, b. 25V, c. 30V, d. 35V, e. 40V and d. 50V.

A heterogeneous sample of MCF10, MCF7, (stained red) and MDA-MB231 (stained green) was introduced into the device using pressure driven flow (Figure 20). As predicted by Figure 19, isolation of MDA-MB231 cells was only possible within a 20kHz range before MCF7 and MCF10A cells were also trapped. To validate the individual results for Figure 20, experiments with the mixed sample were conducted at 30V and at frequencies less than 180kHz. It was found no trapping of the MCF7 and MCF10A cells was successful at 164kHz. This is in agreement with Figure 20.c which predicted DEP response from the MCF7 cell line to begin at 180kHz.

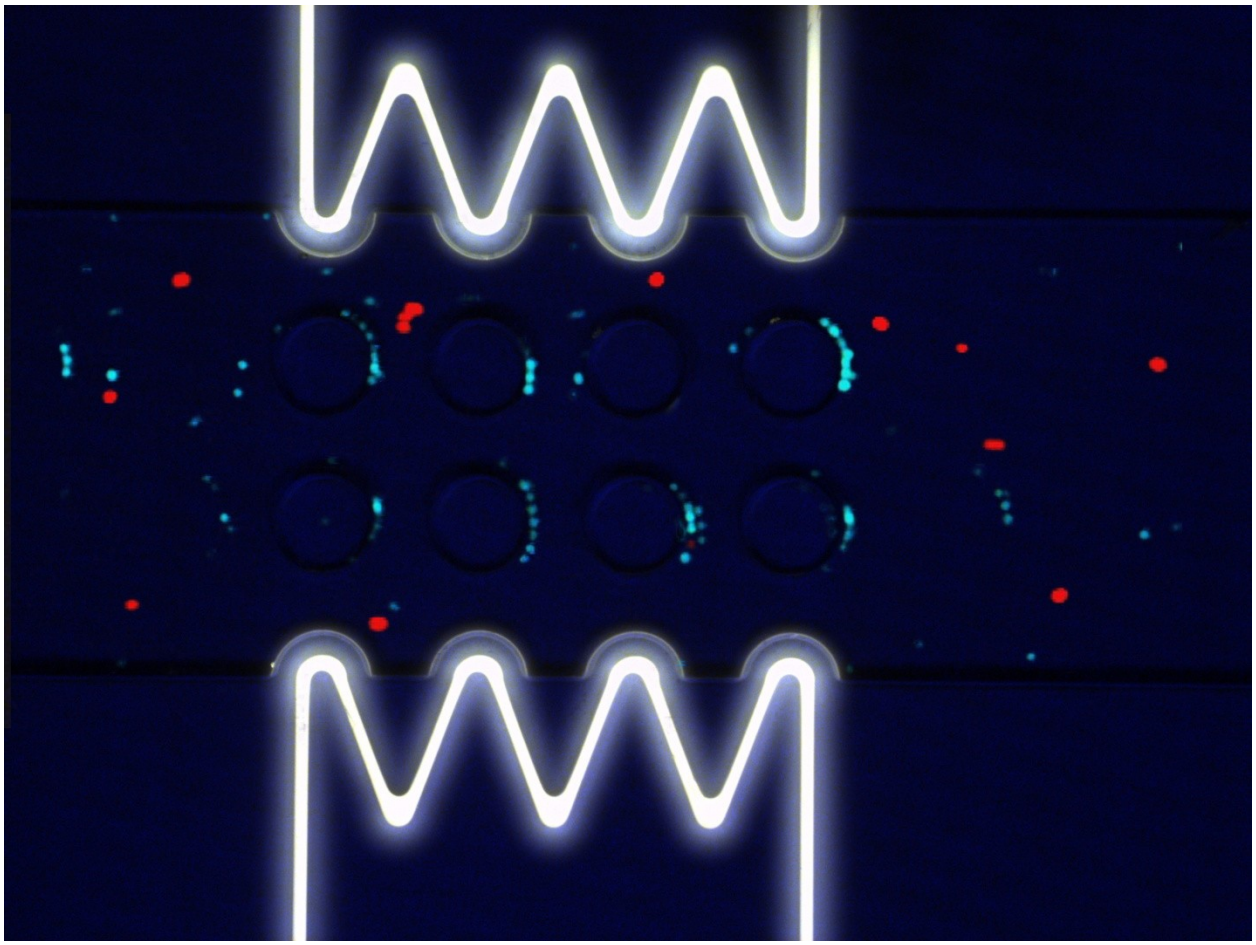

Figure 20: MDA-MB231 cells (green/blue) trapping with no MCF7 or MCF10A trapping. Cells are moving from right to left under pressure driven flow at 30V and 164kHz.

6.2.1 Discussion

While this insulator-based device was unable to isolate MDA-MB231 cells at a high efficiency, differences in the cells were observed supporting the hypothesis that cDEP technology is capable of the isolation of similar cell lines. It is assumed that selectivity has some dependence on the strength of the gradient of the electric field since, in the live/dead investigation, it was found that the insulator based design, which had a much higher electric field gradient, had better selectivity than the noninsulator-based design. It is hypothesized that a device that generates an even larger gradient will therefore have a higher selectivity.

Aside from device design, there are key experimental conditions that can be manipulated in order to provide higher selectivity. Equation 3.23 states the Clausius-Mossotti factor for a cell:

$$K(\omega) = \frac{\omega^2(\tau_M\tau_m - \tau_c\tau_m^{'}) - 1 + j\omega(\tau_m^{'} - \tau_M - \tau_m)}{2 - \omega^2(\tau_c\tau_m^{'} + 2\tau_M\tau_m) + j\omega(\tau_m^{'} + 2\tau_M + 2\tau_m)} \tag{3.23}$$

where τ_c is given as ε_c/σ_c in which ε_c and σ_c are the permittivity and conductivity of the cytoplasm respectively, $\tau_m = C_m R/\sigma_c, \tau_M = \varepsilon_M/\sigma_M$ in which ε_M and σ_M are the perimittivity and conductivity of the medium respectively, and $\tau_m^{'} = C_m R/\sigma_M$. In order to maximize the differences between cells, sample solution conductivity must be adjusted such that these parameters are maximized for one cell type and minimized for another.

While parameter discrepancies for cytoplasm and membrane properties of healthy and cancerous cells may be the basis for experimental data not matching numerical predictions, one major assumption may also hold the key. In modeling specific membrane capacitance, the low-frequency assumption in which conductance is assumed to be zero, C_m becomes a noncomplex scalar. This, however, may not be a valid claim when reaching 10^5 Hz. As previously stated, $C_m = c_m - j\frac{g_m}{\omega}$ where g_m is the membrane conductance. If this term is not neglected C_m becomes a complex term dependent on frequency grossly altering cross-over frequency, and thus, Clausius-Mossotti factor calculations. This variable was investigated in [108] for the dielectric measurement of live and dead cells. Another estimation of membrane capacitance is given by[109]:

$$C_m = \frac{\varepsilon_o \varepsilon_m}{d} x \frac{1 + 2(\frac{d}{D})}{(1 + \frac{d}{D})^2} \tag{6.1}$$

where D is the cell diameter, and d is the membrane thickness. Additionally, variability in cell size must also be accounted for when determining cell DEP response. Since DEP force is highly dependent upon this parameter, variability as small as 1μm could explain numerically why the MCF10A cells should require less DEP force to trap.

6.3 Future Work

The capability to efficiently isolate a cell population would allow for applications such as early detection of exfoliated tumor cells in blood and isolation of transformed cancer cells for treatment screening. In order to achieve this efficiency, device optimization in which the highest possible electric field gradient must be completed. If cDEP alone is unable to attain this goal, there are many possibilities for incorporating other technologies We can employ multi-staged designs initially removing cells with a DEP ratio higher than the targeted cells, concentrate targeted cells and similar healthy cell types, or remove cells with most uniform properties first, and separate target cells from similar healthy cell types. Such serial concentration stages can maintain the desired throughput and increase sensitivity.

Ideally these procedures should be completed using physiological relevant fluids. Additionally, cells must be obtainable once isolated from the sample. Proposed designs include using two syringe pumps to flush out the isolated cells once the electric field is removed (Figure 21). Cells must then be usable for screening conventional and novel chemotherapeutic agents alone or in combination in cell culture. In addition, the detection of tumor cells is a valuable tool to control treatment regimen *in vivo*, identifying changes in geno- and phenotype after treatment and allowing for correction of the treatment regimen if necessary.

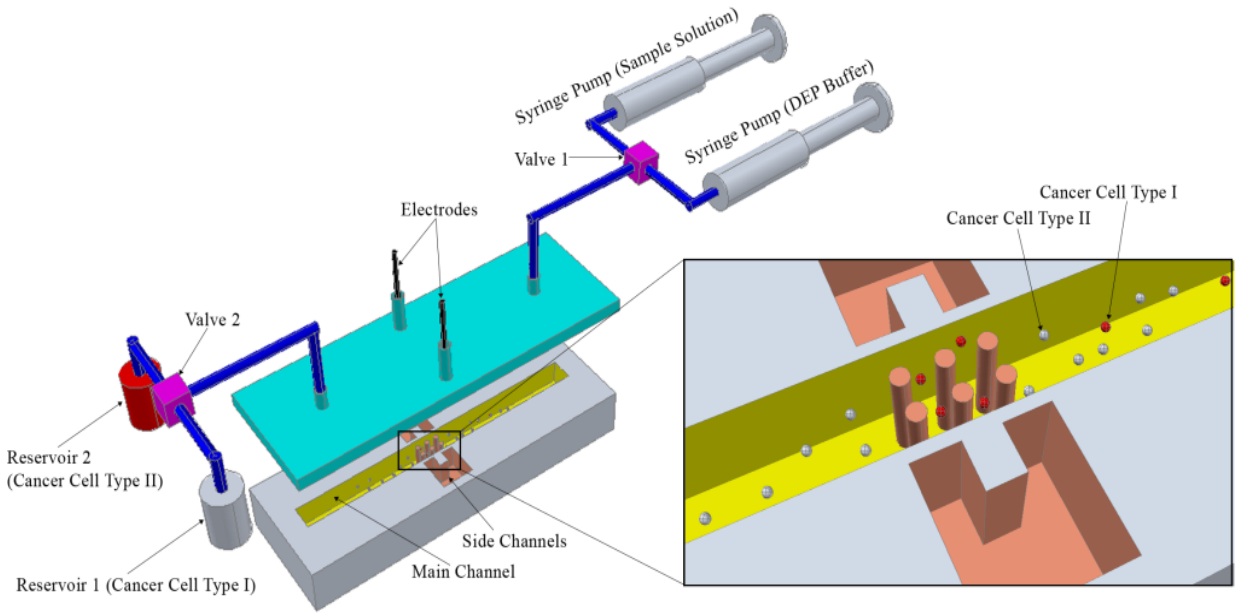

Figure 21: Schematic of future proposed experimental setup.

The potential for cDEP to selectively isolate specific cells from diverse population has been shown in this write-up. The many advantages associated with cDEP give this method great potential for clinical applications among which are: isolation and enrichment for drug screening, treatment therapy, and disease detection.

References

[1] A. Jemal, *et al.*, "Cancer Statistics, 2007," *CA Cancer J Clin,* vol. 57, pp. 43-66, January 1, 2007 2007.

[2] R. A. Smith, *et al.*, "Cancer Screening in the United States, 2007: A Review of Current Guidelines, Practices, and Prospects," *CA Cancer J Clin,* vol. 57, pp. 90-104, March 1, 2007 2007.

[3] E. Banks, *et al.*, "Influence of personal characteristics of individual women on sensitivity and specificity of mammography in the Million Women Study: cohort study," *BMJ,* vol. 329, pp. 477-, August 28, 2004 2004.

[4] A. M. Chiarelli, *et al.*, "Influence of patterns of hormone replacement therapy use and mammographic density on breast cancer detection," *Cancer Epidemiology Biomarkers & Prevention,* vol. 15, pp. 1856-1862, Oct 2006.

[5] B. Mostert, *et al.*, "Circulating tumor cells (CTCs): Detection methods and their clinical relevance in breast cancer," *Cancer Treatment Reviews,* vol. 35, pp. 463-474, Aug 2009.

[6] M. Borgatti, *et al.*, "Antibody-antigen interactions in dielectrophoresis buffers for cell manipulation on dielectrophoresis-based Lab-on-a-chip devices," *Minerva Biotecnologica,* vol. 19, pp. 71-74, Jun 2007.

[7] F. Del Bene, *et al.*, "A model-based approach to the in vitro evaluation of anticancer activity," *Cancer Chemotherapy and Pharmacology,* vol. 63, pp. 827-836, Apr 2009.

[8] T. G. Ntouroupi, *et al.*, "Detection of circulating tumour cells in peripheral blood with an automated scanning fluorescence microscope," *British Journal of Cancer,* vol. 99, pp. 789-795, Aug 2008.

[9] S. V. Sarantseva and A. L. Schwarzman, "Modern genetic approaches to searching for targets for medicinal preparations," *Russian Journal of Genetics,* vol. 45, pp. 761-770, Jul 2009.

[10] D. A. Tatosian and M. L. Shuler, "A Novel System for Evaluation of Drug Mixtures for Potential Efficacy in Treating Multidrug Resistant Cancers," *Biotechnology and Bioengineering,* vol. 103, pp. 187-198, May 2009.

[11] J. F. Leary, *et al.*, "High-throughput cell analysis and sorting technologies for clinical diagnostics and therapeutics," in *Conference on Clinical Diagnostic Systems*, San Jose, Ca, 2001, pp. 16-27.

[12] J. DiRenzo, *et al.*, "Growth factor requirements and basal phenotype of an immortalized mammary epithelial cell line," *Cancer Research,* vol. 62, pp. 89-98, Jan 2002.

[13] I. Osman, *et al.*, "Detection of circulating cancer cells expressing uroplakins and epidermal growth factor receptor in bladder cancer patients," *International Journal of Cancer,* vol. 111, pp. 934-939, Oct 2004.

[14] M. Galan, *et al.*, "Detection of occult breast cancer cells by amplification of CK19 mRNA by reverse transcriptase-polymerase chain reaction: Role of surgical manipulation," *Anticancer Research,* vol. 22, pp. 2877-2884, Sep-Oct 2002.

[15] A. M. C. Dingemans, *et al.*, "Detection of cytokeratin-19 transcripts by reverse transcriptase-polymerase chain reaction in lung cancer cell lines and blood of lung cancer patients," *Laboratory Investigation,* vol. 77, pp. 213-220, Sep 1997.

[16] P. Berteau, *et al.*, "Molecular detection of circulating prostate cells in cancer II: Comparison of prostate epithelial cells isolation procedures," *Clinical Chemistry,* vol. 44, pp. 1750-1753, Aug 1998.

[17] P. Berteau, *et al.*, "Influence of blood storage and sample processing on molecular detection of circulating prostate cells in cancer," *Clinical Chemistry,* vol. 44, pp. 677-679, Mar 1998.

[18] E. Koike, *et al.*, "Endoscopic ultrasonography in patients with thyroid cancer: Its usefulness and limitations for evaluating esophagopharyngeal invasion," *Endoscopy,* vol. 34, pp. 457-460, Jun 2002.

[19] C. P. Schroder, *et al.*, "Detection of micrometastatic breast cancer by means of real time quantitative RT-PCR and immunostaining in perioperative blood samples and sentinel nodes," *International Journal of Cancer,* vol. 106, pp. 611-618, Sep 2003.

[20] S. T. Traweek, *et al.*, "KERATIN GENE-EXPRESSION IN NONEPITHELIAL TISSUES - DETECTION WITH POLYMERASE CHAIN-REACTION," *American Journal of Pathology,* vol. 142, pp. 1111-1118, Apr 1993.

[21] A. A. Adams, *et al.*, "Highly efficient circulating tumor cell isolation from whole blood and label-free enumeration using polymer-based microfluidics with an integrated conductivity sensor," *Journal of the American Chemical Society,* vol. 130, pp. 8633-8641, Jul 2008.

[22] H. A. Pohl, "The Motion and Precipitation of Suspensoids in Divergent Electric Fields," *Journal of Applied Physics,* vol. 22, pp. 869-871, 1951.

[23] H. A. Pohl, "Some Effects of Nonuniform Fields on Dielectrics," *Journal of Applied Physics,* vol. 29, pp. 1182-1188, 1958.
[24] F. F. Becker*, et al.*, "The Removal of Human Leukemia-Cells from Blood Using Interdigitated Microelectrodes," *Journal of Physics D-Applied Physics,* vol. 27, pp. 2659-2662, Dec 1994.
[25] F. F. Becker*, et al.*, "Separation of Human Breast-Cancer Cells from Blood by Differential Dielectric Affinity," *Proceedings of the National Academy of Sciences of the United States of America,* vol. 92, pp. 860-864, Jan 1995.
[26] S. Masuda*, et al.*, "DETECTION OF EXTREMELY SMALL PARTICLES IN THE NANOMETER AND IONIC SIZE RANGE," *Ieee Transactions on Industry Applications,* vol. 24, pp. 740-744, Jul-Aug 1988.
[27] H. Shafiee*, et al.*, "Contactless dielectrophoresis: a new technique for cell manipulation," *Biomed Microdevices,* May 5 2009.
[28] S. Braun and C. Marth, "Circulating tumor cells in metastatic breast cancer - Toward individualized treatment?," *New England Journal of Medicine,* vol. 351, pp. 824-826, Aug 2004.
[29] S. A. Burchill*, et al.*, "Comparison of the RNA-amplification based methods RT-PCR and NASBA for the detection of circulating tumour cells," *British Journal of Cancer,* vol. 86, pp. 102-109, Jan 7 2002.
[30] D. F. Hayes*, et al.*, "Circulating tumor cells at each follow-up time point during therapy of metastatic breast cancer patients predict progression-free and overall survival," *Clinical Cancer Research,* vol. 12, pp. 4218-4224, Jul 2006.
[31] G. T. Budd*, et al.*, "Circulating Tumor Cells versus Imaging--Predicting Overall Survival in Metastatic Breast Cancer," *Clinical Cancer Research,* vol. 12, pp. 6403-6409, November 2006.
[32] M. Cristofanilli*, et al.*, "Circulating tumor cells, disease progression, and survival in metastatic breast cancer," *New England Journal of Medicine,* vol. 351, pp. 781-791, Aug 2004.
[33] Y. Kurusu*, et al.*, "Detection of circulating tumor cells by reverse transcriptase-polymerase chain reaction in patients with resectable non-small-cell lung cancer," *Surgery,* vol. 126, pp. 820-826, Nov 1999.
[34] H. Pohl, "Dielectrophoresis," *Cambridge University Press: Cambridge, 1978.,* 1978.
[35] H. A. Pohl, "Some Effects of Nonuniform Fields on Dielectrics," *J. Appl. Phys. ,* vol. 29, 1958.
[36] M. P. Hughes, "Strategies for dielectrophoretic separation in laboratory-on-a-chip systems," *Electrophoresis,* vol. 23, pp. 2569-2582, Aug 2002.
[37] T. B. Jones, *Electromechanics of Particles*. USA: Cambridge University Press, 1995.
[38] P. R. C. Gascoyne and J. Vykoukal, "Particle separation by dielectrophoresis," *Electrophoresis,* vol. 23, pp. 1973-1983, 2002.
[39] W. M. Arnold and U. Zimmermann, "Rotating-Field-Induced Rotation and Measurement of the Membrane Capacitance of Single Mesophyll-Cells of Avena-Sativa," *Zeitschrift Fur Naturforschung C-a Journal of Biosciences,* vol. 37, pp. 908-915, 1982.
[40] X. B. Wang*, et al.*, "A Unified Theory of Dielectrophoresis and Traveling-Wave Dielectrophoresis," *Journal of Physics D-Applied Physics,* vol. 27, pp. 1571-1574, Jul 14 1994.
[41] W. M. Arnold and U. Zimmermann, "Electro-Rotation - Development of a Technique for Dielectric Measurements on Individual Cells and Particles," *Journal of Electrostatics,* vol. 21, pp. 151-191, Sep 1988.
[42] A. Dussaud, "Particle segregation in suspensions subject to high-gradient ac electric fields," *J Appl Phys,* vol. 88, pp. 5463-5473, 2000.
[43] H. Pohl, "The Motion and Precipitation of Suspensoids in Divergent Electric Fields," *Appl Phys,* vol. 22, pp. 869-871, 1951.
[44] H. Pohl, "Some Effects of Nonuniform Fields on Dielectrics," *Appl Phys,* vol. 29, pp. 1182-1188, 1958.
[45] H. Pohl, *Dielectrophoresis*. Cambridge: Cambridge University Press, 1978.
[46] P. Wong, "Electrokinetics in micro devices for biotechnology applications," *IEEE/ASME Transactions on Mechatronics,* vol. 9, pp. 366-376, 2004.
[47] J. S. Batchelder, "Dielectrophoretic Manipulator," *Review of Scientific Instruments,* vol. 54, pp. 300-302, 1983.
[48] J. Yang*, et al.*, "Cell separation on microfabricated electrodes using dielectrophoretic/gravitational field flow fractionation," *Analytical Chemistry,* vol. 71, pp. 911-918, Mar 1999.
[49] R. Gambari*, et al.*, "Applications to cancer research of "lab-on-a-chip" devices based on dielectrophoresis (DEP)," *Technology in Cancer Research & Treatment,* vol. 2, pp. 31-39, Feb 2003.
[50] F. Becker*, et al.*, "The removal of human leukaemia cells from blood using interdigitated microelectrodes," *J. Phys. D: Appl. Phys,* vol. 27, pp. 2659-2662, 1994.
[51] P. Gascoyne*, et al.*, "Dielectrophoretic Separation of Cancer Cells from Blood," *IEEE Trans. Industry Applications,* vol. 33, pp. 670-678, 1997.

[52] Y. Huang, *et al.*, "Dielectrophoretic cell separation and gene expression profiling on microelectronic chip arrays," *Anal Chem,* vol. 74, pp. 3362-3371, 2002.
[53] J. Cheng, *et al.*, "Preparation and hybridization analysis of DNA/RNA from E. coli on microfabricated bioelectronic chips," *Nat Biotechnol,* vol. 16, pp. 541-546, 1998.
[54] M. Stephens, *et al.*, "The dielectrophoresis enrichment of CD34+ cells from peripheral blood stem cell harvests," *Bone Marrow TRansplant,* vol. 18, pp. 777-782, 1996.
[55] Y. Huang, *et al.*, "Introducing dielectrophoresis as a new force field for field-flow fractionation," *Biophys J,* vol. 73, pp. 1118-1129, 1997.
[56] U.-J. Kim, *et al.*, "Selection of mammalian cells based on their cell-cycle phase using dielectrophoresis," *Proc Natl Acad Sci,* vol. 104, pp. 20708-20712, 2007.
[57] S. Masuda, *et al.*, "Detection of extremely small particles in the nanometer and ionic size range," *IEEE Trans. on Industry Applications,* vol. 24, pp. 740-744, 1988.
[58] B. H. Lapizco-Encinas, *et al.*, "Insulator-based dielectrophoresis for the selective concentration and separation of live bacteria in water," *Electrophoresis,* vol. 25, pp. 1695-1704, Jun 2004.
[59] B. H. Lapizco-Encinas, *et al.*, "Dielectrophoretic concentration and separation of live and dead bacteria in an array of insulators," *Analytical Chemistry,* vol. 76, pp. 1571-1579, Mar 15 2004.
[60] B. Simmons, *et al.*, "Polymeric insulator-based (electrodeless) dielectrophoresis (iDEP) for the monitoring of water-borne pathogens," *Micro Total Analysis Systems 2004, Vol 2,* pp. 171-173
[61] B. H. Lapizco-Encinas, *et al.*, "An insulator-based (electrodeless) dielectrophoretic concentrator for microbes in water," *Journal of Microbiological Methods,* vol. 62, pp. 317-326, 2005.
[62] E. B. Cummings, *et al.*, "Fast and selective concentration of pathogens by insulator-based dielectrophoresis," *Abstracts of Papers of the American Chemical Society,* vol. 230, pp. U404-U405, Aug 28 2005.
[63] G. J. McGraw, *et al.*, "A Comparison of Insulator-Based Dielectrophoretic Devices for the Monitoring and Separation of Waterborne Pathogens as a Function of Microfabrication Technique," *Antiterrorism and Homeland Defense: Polymers and Materials,* vol. 980, pp. 133-157
[64] S. Ozuna-Chacon, *et al.*, "Insulator-based dielectrophoresis," *Revista Mexicana De Ingenieria Quimica,* vol. 6, pp. 329-335, Dec 2007.
[65] B. H. Lapizco-Encinas, *et al.*, "Insulator based dielectrophoresis: Effects of bulk medium properties," *Icnmm2007: Proceedings of the 5th International Conference on Nanochannels, Microchannels, and Minichannels,* pp. 177-183
[66] J. P. Wang, *et al.*, "Numerical analysis and optimization of insulator-based dielectrophoresis devices for cell sorter applications," *2007 2nd IEEE International Conference on Nano/Micro Engineered and Molecular Systems, Vols 1-3,* pp. 814-817
[67] F. Du, *et al.*, "Insulator-based dielectrophoresis in viscous media - Simulation of particle and droplet velocity," *Journal of Electrostatics,* vol. 65, pp. 452-458, Jun 2007.
[68] R. V. Davalos, *et al.*, "Performance impact of dynamic surface coatings on polymeric insulator-based dielectrophoretic particle separators," *Analytical and bioanalytical chemistry,* vol. 390, pp. 847-855, Feb 2008.
[69] B. H. Lapizco-Encinas, *et al.*, "Protein manipulation with insulator-based dielectrophoresis and direct current electric fields," *Journal of Chromatography A,* vol. 1206, pp. 45-51, Oct 3 2008.
[70] S. Ozuna-Chacon, *et al.*, "Performance characterization of an insulator-based dielectrophoretic microdevice," *Electrophoresis,* vol. 29, pp. 3115-3122, Aug 2008.
[71] C. P. Jen, *et al.*, "Cell Trapping Utilizing Insulator-based Dielectrophoresis in The Open-Top Microchannels," *Dtip 2008: Symposium on Design, Test, Integration and Packaging of Mems/Moems,* pp. 289-291
[72] C. P. Jen, *et al.*, "Hydrodynamic Separation of Cells Utilizing Insulator-based Dielectrophoresis," *Dtip 2009: Symposium on Design, Test, Integration and Packaging of Mems/Moems,* pp. 55-59
[73] C. P. Jen and T. W. Chen, "Selective trapping of live and dead mammalian cells using insulator-based dielectrophoresis within open-top microstructures," *Biomedical Microdevices,* vol. 11, pp. 597-607, Jun 2009.
[74] H. Shaflee and R. V. Davalos, "An Autonomous Cell Type Selective Irreversible Electroporation Microsystem Using Insulator Based Dielectrophoresis (Idep)," *Proceedings of the Asme Summer Bioengineering Conference 2008, Pts a and B,* pp. 591-592
[75] A. Lambrechts, *et al.*, "The actin cytoskeleton in normal and pathological cell motility," *International Journal of Biochemistry & Cell Biology,* vol. 36, pp. 1890-1909, Oct 2004.

[76] A. Lostumbo, *et al.*, "Flow cytometry: A new approach for the molecular profiling of breast cancer," *Experimental and Molecular Pathology,* vol. 80, pp. 46-53, 2006.
[77] S. Nagrath, *et al.*, "Isolation of rare circulating tumour cells in cancer patients by microchip technology," *Nature,* vol. 450, pp. 1235-U10, Dec 2007.
[78] J. Cheng, *et al.*, "Isolation of cultured cervical carcinoma cells mixed with peripheral blood cells on a bioelectronic chip," *Anal Chem,* vol. 70, pp. 2321-2326, 1998.
[79] L. Altomare, *et al.*, "Levitation and movement of human tumor cells using a printed circuit board device based on software-controlled dielectrophoresis," *Biotechnol Bioeng,* vol. 82, p. 474, 2003.
[80] A. Griffith and J. Cooper, "Single-cell measurements of human neutrophil activation using electrorotation," *Anal Chem,* vol. 70, pp. 2607-2612, 1998.
[81] M. Toner and D. Irimia, "Bone-on-a-chip," *Ann Rev Biomed Eng,* vol. 7, pp. 77-103, 2005.
[82] P. R. C. Gascoyne, *et al.*, "Dielectrophoretic Separation of Mammalian-Cells Studied by Computerized Image-Analysis," *Measurement Science & Technology,* vol. 3, pp. 439-445, May 1992.
[83] P. R. C. Gascoyne, *et al.*, "Dielectrophoretic separation of cancer cells from blood," *Ieee Transactions on Industry Applications,* vol. 33, pp. 670-678, May-Jun 1997.
[84] X. B. Wang, *et al.*, "Cell separation by dielectrophoretic field-flow-fractionation," *Analytical Chemistry,* vol. 72, pp. 832-839, Feb 2000.
[85] J. Vykoukal, *et al.*, "Enrichment of putative stem cells from adipose tissue using dielectrophoretic field-flow fractionation," *Lab on a Chip,* vol. 8, pp. 1386-1393, Aug 2008.
[86] P. Sabounchi, *et al.*, "Sample concentration and impedance detection on a microfluidic polymer chip," *Biomedical Microdevices,* vol. 10, pp. 661-670, Oct 2008.
[87] C. P. Jen and T. W. Chen, "Trapping of cells by insulator-based dielectrophoresis using open-top microstructures," *Microsystem Technologies-Micro-and Nanosystems-Information Storage and Processing Systems,* vol. 15, pp. 1141-1148, Aug 2009.
[88] H. Shafiee, *et al.*, "Contactless Dielectrophoresis: A New Technique For Cell Manipulation," *Biomedical Microdevices,* 2009.
[89] T. B. Jones, "Basic theory of dielectrophoresis and electrorotation," *Ieee Engineering in Medicine and Biology Magazine,* vol. 22, pp. 33-42, 2003.
[90] H. A. Pohl and J. S. Crane, "Dielectrophoresis of Cells," *Biophys. J.,* vol. 11, pp. 711-727, September 1, 1971 1971.
[91] H. Morgan and N. G. Green, *AC Electrokinetics: Colloids and Nanoparticles*. Hertfordshire, England: Research Studies Press LTD, 2003.
[92] H. Morgan, *et al.*, "Single Cell Dielectric Spectroscopy," *Journal of Physics D: Applied Physics,* vol. 40, 2007.
[93] K. V. I. S. Kaler and T. B. Jones, "Dielectrophoretic Spectra of Single Cells Determined by Feedback-Controlled Levitation," *Biophysical Journal,* vol. 57, pp. 173-182, Feb 1990.
[94] A. Docoslis, *et al.*, "A novel dielectrophoresis-based device for the selective retention of viable cells in cell culture media," *Biotechnol Bioeng,* vol. 54, pp. 239-50, May 5 1997.
[95] X. J. Wang, *et al.*, "General expressions for dielectrophoretic force and electrorotational torque derived using the Maxwell stress tensor method," *Journal of Electrostatics,* vol. 39, pp. 277-295, Aug 1997.
[96] L. A. Flanagan, *et al.*, "Unique dielectric properties distinguish stem cells and their differentiated progeny," *Stem Cells,* vol. 26, pp. 656-665, 2008.
[97] K. V. Kaler, *et al.*, "Dual-frequency dielectrophoretic levitation of Canola protoplasts," *Biophysical Journal,* vol. 63, pp. 58-69, Jul 1992.
[98] D. Holmes and H. Morgan, "Cell sorting and separation using dielectrophoresis," *Electrostatics 2003,* pp. 107-112, 2004.
[99] A. Han, *et al.*, "Quantification of the heterogeneity in breast cancer cell lines using whole-cell impedance spectroscopy," *Clinical Cancer Research,* vol. 13, pp. 139-143, Jan 1 2007.
[100] R. P. Joshi, *et al.*, "Energy-landscape-model analysis for irreversibility and its pulse-width dependence in cells subjected to a high-intensity ultrashort electric pulse," *Phys Rev E Stat Nonlin Soft Matter Phys,* vol. 69, p. 051901, May 2004.
[101] I. Ermolina, *et al.*, "Study of normal and malignant white blood cells by time domain dielectric spectroscopy," *Ieee Transactions on Dielectrics and Electrical Insulation,* vol. 8, pp. 253-261, Apr 2001.
[102] F. F. Becker, *et al.*, "Separation of human breast cancer cells from blood by differential dielectric affinity," *Proc Natl Acad Sci U S A,* vol. 92, pp. 860-4, Jan 31 1995.

[103] I. Zudans, *et al.*, "Numerical calculations of single-cell electroporation with an electrolyte-filled capillary," *Biophysical Journal,* vol. 92, pp. 3696-3705, May 10 2007.
[104] H. Shafiee, *et al.*, "Selective isolation of live/dead cells using contactless dielectrophoresis (cDEP)," *Lab on a Chip,* pp. -, 2010.
[105] K. H. Kang, *et al.*, "Effects of dc-dielectrophoretic force on particle trajectories in microchannels," *Journal of Applied Physics,* vol. 99, Mar 2006.
[106] J. Zhu and X. Xuan, "Dielectrophoretic focusing of particles in a microchannel constriction using DC-biased AC flectric fields," *Electrophoresis,* vol. 30, pp. 2668-75, Aug 2009.
[107] M. S. H Shafiee, P Zellner, M Agah, RV Davalos, "A new strategy for sample concentration and enrichment: Contactless Dielectrophoresis," in *AIChE Annual Meeting*, Nashville,TN, 2009.
[108] P. Patel and G. H. Markx, "Dielectric measurement of cell death," *Enzyme and Microbial Technology,* vol. 43, pp. 463-470, Dec 10 2008.
[109] T. Hanai, *et al.*, "Method for Determining Dielectric-Constant and Conductivity of Membrane-Bounded Particles of Biological Relevance," *Biophysics of Structure and Mechanism,* vol. 1, pp. 285-294, 1975.